AB-INITIO CALCULATIONS OF HIGH PRESSURE PHASE TRANSITION, STRUCTURAL AND ELECTRONIC PROPERTIES OF $Be_XZn_{1-X}S$ (X = 0.00, 0.41, 0.66 AND 1.00) TERNARY ALLOYS

FATANA FUFA

A THESIS SUBMITTED TO THE SCHOOL OF GRADUATE STUDIES OF ADDIS ABABA UNIVERSITY IN PARTIAL FULFILLMENT OF THE REQUIREMENTS FOR THE DEGREE OF MSc IN MATERIALS SCIENCE

ADDIS ABABA UNIVERSITY

ADDIS ABABA, ETHIOPIA

June, 2013

ADDIS ABABA UNIVERSITY

SCHOOL OF GRADUATE STUDIES

This is to certify that the thesis prepared by Fatana Fufa Bakare entitled: "*Abinitio calculations of high Pressure phase transition, structural and electronic properties of* $Be_XZn_{1-X}S$ *(*X = *0.00, 0.41, 0.66 and 1.00) ternary alloys*" and submitted in partial fulfillment of the requirements for the Degree of Master of Science in Materials Science complies with the regulations of University and meets the accepted standards with respect to originality and quality.

Signed by the Examining Committee:

External Examiner: Ahmed Mustefa (PhD) Signature _____ Date _____

Internal Examiner: Teketel Yohanis (Professor) Signature _____ Date 04/07/2013

Advisor: Javed Mazher (Professor) Signature _____ Date 04/07/2013

_____

Chair of Department or Graduate Program Coordinator

ACKNOWLEDGEMENTS

First of all, this acknowledgement will not be complete without mentioning the Almighty GOD for his love and mercy.

I would like to express my sincere gratitude to Prof. Javed Mazher for being such an extraordinary supervisor. His unique and genuine enthusiasm for science kept me motivated during every step of my MSc, and in addition to supporting my core research activities he took the time and interest to educate me on a wide variety of other aspects about the scientific community and what it takes to succeed. I could not imagine a better MSc experience than having the privilege to work with and learn from Prof. Javed Mazher.

Then my gratitude goes to Prof. Teketel Yohannes, Chair of Materials Science Program college of Natural Sciences Addis Ababa University for motivating and following on my research activities.

Last but not least, I am deeply indebted to my friends and students of materials science program Gebrekirstos Gebreamlak, Mesfin Haile, Asegidew Ergete, Girma Erjabo and Gebregzabher Gebretsadkan for their help and moral support.

Finally, I thank my family specially Hawwi Negasa for her love and support, without which I would never have got here in the first place.

ABSTRACT

Ab-initio Calculations of High Pressure Phase Transition, Structural and Electronic Properties of $Be_xZn_{1-x}S$ (x = 0.00, 0.41, 0.66 and 1.00) Ternary Alloys

Fatana Fufa

Addis Ababa University, 2013

In this piece of research, we have performed self-consistent ab-initio calculations to study the structural and electronic properties of $Be_XZn_{1-X}S$ mixed crystals in the various low and high pressure crystallographic phases of the alloy. The zinc blend phase and rock salt phase of compositionally variant zinc-beryllium-sulfide have been used for the calculations of structural and electronic properties within the local density approximation of density functional theory. The concentration of Be (X) changes from 0.00, 0.41, and 0.66 to 1.00 in the alloy. Super cells (54 atoms) of the alloys are constructed and fully relaxed. All the values of ternary and binary alloy lattice constants, bulk modulus and energy band gap are calculated on these relaxed structures. Our results are comparable to the contemporary theoretical and experimental observations. Our values for the structural parameters obtained in the LDA approximation are also in good agreement with the experimental values. We have also observed direct band to indirect band gap ($\Gamma \rightarrow \Gamma$) $\rightarrow$ ($\Gamma \rightarrow X$) by increasing beryllium concentrations along with some LDA related under estimations of gap widths. For all the samples of the alloy, high pressure phase transitions are found to present and reported in the range of giga pascal pressures. At the same time, increase of hardening of the alloy is reported due to Be content and the bulk modulus correspondingly increases in the alloy. We have also analyzed the concentration related effects on electronic density of states and bowing parameters.

TABLE OF CONTENTS

LIST OF FIGURES

LIST OF TABLES

LIST OF ABBREVIATION

Be	Beryllium
BZ	Brillouin Zone
DFT	Density Functional Theory
DOS	Density of States
GGA	Generalized Gradient Approximation
LDA	Local Density Approximation
SCF	Self-Consistent Field
XC	Exchange and Correlation
b	Bowing parameter
FCC	Face centre cubic
GUI	Graphic user interface
VD	Volume deformation
CE	Charge exchange
SR	Structural relaxation
FP-LAPW	Full polarized linearized Argument plane wave
B_1	Rock salt
B_3	Zinc blende
FWHM	Full width half maximum

CHAPTER 1 INTRODUCTION

The current state of art in the field of computer simulations has become increasingly powerful tool for studying materials properties and their physical behaviors. The first principles quantum methods generally give the increasingly accurate results for the applied problems related to large simulations' system sizes. Semiconductor materials science provides some important input for science and technology. This field studies material properties from the nanoscale to the macroscopic level, experimentally and theoretically. The wide band gap II-VI semiconductors have been regarded as promising materials for the fabrication of visible light emitting devices for decades. ZnS is the prototype II-VI semiconductors and their cubic phase, which occurs naturally as a mineral, has been called the zinc blende structure. On the theoretical side, many authors have studied these semiconductors to explore their electronic properties, using various computational methods [1]. The major drawback in the pure II-VI compound semiconductors have defect propagation due to the soft nature of the semiconductor which arises from its ionicity. However, Be alloying of ZnS can increase its device performance that result from the covalent character of the BeS. Besides, the ternary compounds have many advantages over binary compounds: ZnS and ZnSe, because the lattice constant, the bulk modulus, band gap and optical properties can be tuned just by changing the concentration of the dopant [1]. In recent years, several theoretical and experimental studies have focused on the electronic properties of ZnS semiconductor largely motivated by the potential applications of these materials in opto-electronic devices, particularly blue-green lasers and in technological applications mainly in the field of optical devices [2]. In particular, the physical properties of II–VI mixed crystals of binary compounds with Be chalcogenides are of significant interest for their potential applications in the technology of green semiconductor lasers [3]. The II–VI compounds semiconductors have been

the subject of extensive research both in fundamental studies and for potential applications in devices. The broad range of band gaps and lattice constants available from these materials, and the unique fundamental phenomena they exhibit make them attractive for a wide range of applications such as infrared lasers and detectors, blue green lasers and light emitting diodes (LEDS). There are some hopes that ZnS based structures will be good for such applications [4]. Motivated by the above factors, we have instigated this piece of research by taking alloy of different concentrations. The first chapter deals with the literature survey of ZnS, BeS and mixed alloy ternary systems. The current trends and the contemporary scientific research are discussed in detail for the pressure and concentration dependent structural and electronic properties of these systems. Objectives of the thesis are explained in the second chapter. The computational review for the DFT theory and its implementation is briefly explained in the third chapter. Followed by this, the simulation methodology and the theoretical DFT parameters used for the calculations in this thesis are discussed in chapter four. High pressure phase transitions, changes in lattice constants with the beryllium concentration and its effects on the electronic band structure and density of states are presented and analyzed in the light of existing theory in the subsequent chapters of results, discussions and conclusions.

1.1. Literature Review

1.1.1. Zinc sulfide semiconductor

Zinc sulfide (or zinc sulphide) is an inorganic compound with the chemical formula of ZnS. This is the main form of zinc found in nature, where it mainly occurs as the mineral sphalerite. ZnS exists in two main crystalline forms, and this dualism is often a main example of polymorphism. In both polymorphisms, the coordination geometry at Zn and S are tetrahedral. The more stable

cubic form is known also as zinc blende (B3) or sphalerite. The hexagonal form is known as the mineral wurtzite (B4). The transition from the sphalerite form to the wurtzite form occurs at around 1020 ^{0}C . Zinc sulfide (ZnS) as a typical II–VI semiconductor compound with wide direct band gap energy of (3.6 eV) semiconductor at room temperature and has been used as an important material for ultraviolet light-emitting diodes and injection lasers, flat panel displays, electroluminescent devices, antireflection coating for heterojunction solar cells photovoltaic cells which enable wide application in the field of displays, sensors and lasers and infrared (IR) windows [5 - 7]. At a high pressure, both of them can transform into rock salt (NaCl) structure (B1). Recently, it was reported phase transition of nano ZnS powder as a function of pressure [8, 9].

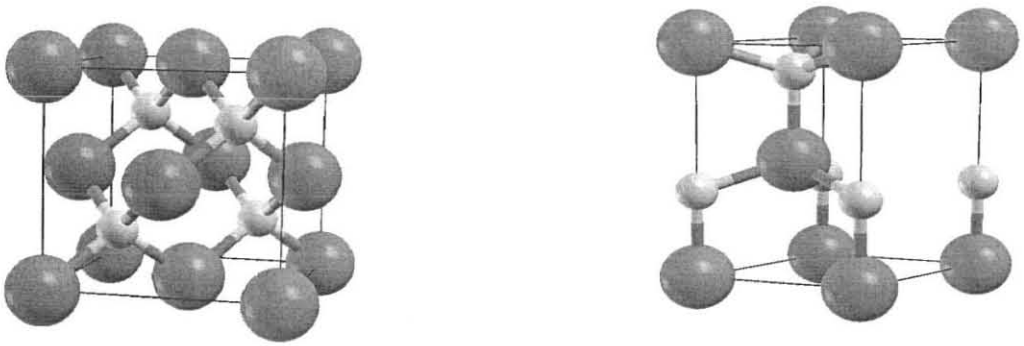

Figure 1. Zinc blende (left) and Wurtzite (right) crystal structures of zinc sulfide, the large ball is zinc and the small balls represent sulfur atom.

1.1.2. Beryllium sulfide semiconductor

The groups II–VI beryllium chalcogenides such as BeS, BeSe, and BeTe and their alloys have attracted both scientific and technological interest in recent years. At ambient conditions the thermodynamically stable phase of BeS, BeSe and BeTe are the cubic zinc blende structure. The beryllium chalcogenides show interesting features. They are characterized by a strong covalent

character of their chemical bonding, short bond length and large hardness. It has been suggested that optoelectronic devices based on beryllium chalcogenides have advantage over most of II–VI semiconductors devices due to their high p- type doping concentrations and long lifetimes [10]. Beryllium chalcogenides are considered to be promising materials for optoelectronic devices in the blue and UV spectral region because of their high band gap energies. Besides the above applications, Be chalcogenides also provide interesting aspects for fundamental physics investigation because they exhibit covalent bonding and reduced band polarity, which are unique among II–VI compounds [4]. There has also been a growing interest in the study of these materials under high pressure conditions, motivated by the need of synthesizing new solids with targeted physical properties. In this context, beryllium chalcogenides BeX (X = S, Se, Te), which exhibit covalent bonding, are potentially attractive materials for technological applications because they have very large band gaps, and they are interesting for blue–green laser diodes and laser emitting diodes [11]. In the other hand, these compounds have similar structure and bonding with the group III–IV semiconductors in particular the boron compounds BN, BP, BAs and BSb in having the same crystal structure, large band gaps (2.7 – 5.5 eV) and high value of the bulk modulus [12, 13]. The lattice constant of BeS and BeTe are close to those of GaAs and ZnSe [14].

1.1.3. Mixed II–VI semiconductor alloys

The II–VI compounds semiconductors have been the subject of extensive research both in fundamental studies and for potential applications in devices. The broad range of band gaps and lattice constants available from these materials, and the unique fundamental phenomena they exhibit, make them attractive for a wide range of applications such as infrared lasers and detectors, blue-green lasers and light emitting diodes (LEDS) [15]. There are some hopes that

ZnS based structures will be good for such applications. Hence, the use of Be in ZnX based ternary alloys such $Be_XZn_{1-X}S$ and $Be_XZn_{1-X}Se$ should be useful for increasing the hardness of the material and for decreasing degradation rates, which is important for improved device lifetime [16 - 18]. ZnBeS alloys are of a particular interest since by varying the concentration in $Be_XZn_{1-X}S$, a wide range of band energies can be covered. The possible development of heterostructures based on these new material systems needs a detailed investigation of these alloys. On the theoretical side, there are few works on these compounds concerning structural and electronic properties [19, 20]. In order to complete these exciting works and to provide a basis for understanding future device applications, we have employed (DFT) to some properties of $Be_XZn_{1-X}S$ alloy.

1.1.4. Electronic properties of a $Be_XZn_{1-X}S$ alloy

The atomic structure of an alloy is important for understanding its properties, in which bond length relaxation and the lattice constant are the key parameters. Theories of bond length relaxation and the lattice constant in alloys were put forward by Pauling and Vegard's a long time ago. Pauling noted that the bond lengths in an alloy are the sum of their constituent element atomic radii, i.e. the bond lengths are independent of the alloy concentration. Vegard's discovered that the lattice constant is approximately equal to the composition weighted average of the lattice constants of the pure materials, i.e. the lattice constant is dependent on the alloy concentration [21]. Usually, in the treatment of alloys, it is assumed that the atoms are located at the ideal lattice sites and the lattice constant varies linearly with concentration X according to the so-called Vegard's law [22].

$$a(A_XB_{1-X}C) = Xa_{AC} + (1 - X)a_{BC} \quad (1)$$

Where aAC and aBC are the equilibrium lattice constants of the binary compounds AC and BC Hence, the lattice constant can be written as:

$$a(A_XB_{1-X}C) = Xa_{AC} + (1 - X)a_{BC} - X(1 - X)b \quad (2)$$

Where, the quadratic term b is the bowing parameter. In order to better understand the physical origins of the large and concentration dependent bowing in $Be_XZn_{1-X}S$ alloys, we follow the procedure of Bernard and Zunger [22] and decompose the total bowing parameter b into physically distinct contributions. The overall bowing coefficient at a given average concentration X measures the change in band gap according to the formal reaction.

$$XBeS(aBeS) + (1 - X)ZnS(aZnS) \rightarrow Be_XZn_{1-X}S(a_{eq}) \quad (3)$$

Where, aBeS and aZnS are the equilibrium lattice constants of the binary compounds and a_{eq} is the equilibrium lattice constant of the alloy with the average concentration X. We decompose reaction into three steps:

$$BeS(aBeS) + ZnS(aZnS) \rightarrow BeS(a) + ZnS(a) \quad (4)$$

$$XBeS(a) + (1 - X)ZnS(a) \rightarrow Be_XZn_{1-X}S(a) \quad (5)$$

$$Be_XZn_{1-X}S(a) \rightarrow A_XB_{1-X}C(a_{eq}) \quad (6)$$

The first contribution, the volume deformation represents the relative response of the band structure of the binary compounds AC and BC to hydrostatic pressure. The second contribution, the charge-exchange contribution, reflects a charge transfer effect that is due to the different (averaged) bonding behavior at the lattice constant a. The final step measures by, changes due to

the structural relaxation in passing from the unrelaxed to the relaxed alloy. Consequently, the total gap bowing parameter is defined as:

$$b = b_{VD} + b_{CE+}b_{SR} \tag{7}$$

The general representation of the concentration dependent band gap of the alloys in terms of binary compounds gaps of the, $E_{AC}(a_{AC})$, $E_{BC}(a_{BC})$ and the total bowing parameter b is:

$$E_g(X) = xE_{AC}(a_{AC}) + (1 - X)E_{BC}(a_{BC}) - bX(1 - X) \tag{8}$$

Where VD, CE and SR represents respectively the volume deformation effect, the charge exchange contribution and the structural relaxation of the alloy according to the following expressions:

$$b_{VD} = \frac{E_{BeS(aBeS)} - E_{BeS(a)}}{1-X} + \frac{E_{ZnS(aZnS)} - E_{ZnS(a)}}{X} \tag{9}$$

$$b_{CE} = \frac{E_{BeS(a)}}{1-X} + \frac{E_{ZnS(a)}}{X} - \frac{E_{Be_XZn_{1-X}S(a)}}{X(1-X)} \tag{10}$$

$$b_{SR} = \frac{E_{Be_XZn_{1-X}S(a)} - E_{Be_XZn_{1-X}S(a_{eq})}}{X(1-X)} \tag{11}$$

All these energy gaps occurring in Expressions 9, 10 and 11 have been calculated for the indicated atomic structures and lattice constants.

1.1.5. Direct and indirect gap Materials

The inter band absorption rate depends on the band structure of the semiconductor. The band structure or E (k) diagram of a semiconductor is a plot of the total energy of an electron as a function of electron wave vector within some region of the Brillouin zone. We have two types of semiconductor band gap; direct and indirect [23, 24].

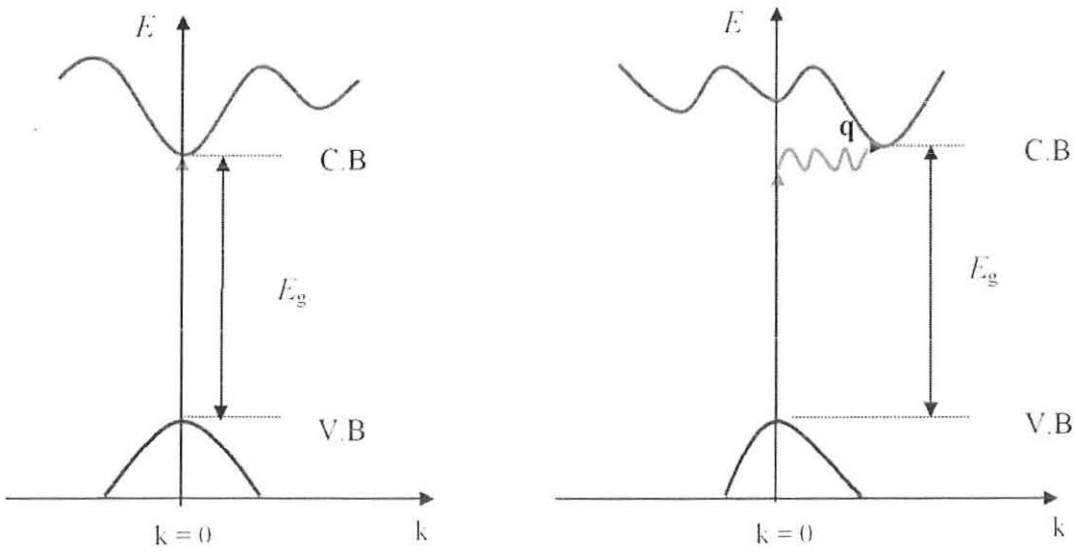

Figure 2. Shows the E (k) diagram of a direct and an indirect band gap material.

In a direct gap semiconductor, the valence band maximum and conduction band minimum occur at the zone center where k = 0. Hence, there is no net transfer of momentum associated with the inter band transition in a direct band gap semiconductor. If the valence band maximum and conduction band minimum do not occur at k = 0 in k space, then an inter band transition must involve a phonon to conserve momentum, and the material is called an indirect gap semiconductor. In this project, we focus on the Be concentration whether the materials have direct or indirect band gap through the Be concentrations at (X = 0.00, 0.41, 0.66, and 1.00).

1.1.6. Effect of pressure on the structural properties of $Be_XZn_{1-X}S$ alloy

The II–VI compounds have received and still receive considerable interest because of their potential technological applications. The first experimental study of the structural phase transformations of II–VI materials under high pressure was conducted about forty years ago by Edwards and Drickamer [25]. Since then, this subject has attracted a lot of attention. The generally accepted view was that these compounds transform under high pressure from zinc-blende (ZB) or wurtzite to rock salt (RS). However, recent experiments performed by using angle-dispersive X-ray techniques for many II–VI, III–V and group IV semiconductors have altered significantly their widely accepted structural systematic [26]. New low symmetry phases have been observed, such as the cinnabar phase in CdTe , ZnTe and GaAs form in many II–VI and III–V compounds [25] simple cubic with atom basis, the binary analog of is observed in Si and Ge structure in GaAs [27]. The latter structure has also been observed in some I–VII compounds, namely CuCl and CuBr [26]. The study of phase transitions under pressure is not only of interest for practical materials research, but it offers a rich playground in physics: group theory, basic electronic structure theory, lattice dynamics, and transport. To practice relations between different phases is a fine exercise in the group theory; electronic properties exhibit effects of extreme (de) localization and certain lattice vibrations may indicate a (kinetic) way into a new phase. This playground is very vast; the present work deals only with some semiconductor structures, addressing only some aspects of their electronic structure. Zinc sulphide crystallizes under normal conditions with the zinc-blende (ZB) structure, in the four fold coordinated. As the pressure is applied to ZnS it transforms into rock salt phase (NaCl) with six fold coordinated reported a transition pressure of, 14.5 GPa although later studies have placed it at a somewhat higher pressure and 15.5 GPa. In contrast to zinc blende structure, the NaCl phase is found to an

indirect-gap semiconductor which has been confirmed by first principles calculations. The high pressure behavior of ZnS has been the subject of several recent theoretical and experimental studies [2]. Measure of the deformations is depending on elastic stiffness coefficients that is a very important characterization of the crystals under varying pressure. Moreover, the elastic constants of the materials at high pressures are essential in order to predict and understand material response, strength, mechanical stability and phase transitions. However, only, a few studies have conducted on the mechanical properties of ZnS at elevated pressures, as well as pressure dependence of its elastic constants, so far. The accurate measurement of these quantities is a difficult task due to difficult experimental conditions at high pressure. With the advances in ab initio methods, it is possible to compute a systematic study of the elastic properties as well as electronic and structural properties of materials at elevated pressure conditions. ZnS crystallizes in the cubic zincblende (B3) and wurtzite (B4) structures at ambient pressure. There is a phase transition from B4 structure to B3 structure and from B3 structure to B1 (rock salt) structure when the pressure is applied [28, 29].

1.1.7. Murnaghan equation of state

Francis D. Murnaghan of John Hopkins University developed the Murnaghan Equation of state [30 – 32] for the calculation of elastic constants of the material like bulk modulii with the help of pressure response and now a day this equation is widely used for the calculation of applied pressure with the help of changes in structural volumes during phase transitions. He presented an equation of state suitable for representing solids. It is to be noted that volume and total energy have interdependence and thus the equation of state has found considerable use in the condensed phase media. Three derivative relations are mostly utilized to lead to the final formulation, namely:

$$P = -\left(\frac{\partial E}{V}\right) S \tag{12}$$

$$B0 = -V\left(\frac{\partial P}{\partial V}\right) T \tag{13}$$

$$B' = \left(\frac{\partial B}{\partial P}\right) T \tag{14}$$

Where P is the pressure, E is the internal energy, V is the volume, B0 is the bulk modulus, and B' is the pressure derivative of the bulk modulus at constant temperature. Making the assumption that B' is a constant allows one to assign a linear dependence of the bulk modulus on the pressure, which allows specifying the single bulk modulus as a variant, while the derivative, B' represented as the materials constant. This leads to a relationship for pressure:

$$P = \frac{B0}{B\prime}\left[\left(\frac{V0}{V}\right) B' - 1\right] \tag{15}$$

That can be integrated to represent the change in the energy of the solid with respect to the elastic constants or the pressure.

$$E = E_0 + \frac{1}{2} B0 \frac{(V-V0)^2}{V0} \tag{16}$$

Where, E(V) is the total energy at cell volume V, E(V0) is the total energy at equilibrium volume V0 (at P = 0). In the present work, the elastic constants of the alloy have been calculated by Equation 16 of the Murnaghan Equation of state. For a given equation of state (EOS), which expresses the energy 'E' as a function of the lattice parameter 'a' or volume 'V' the bulk modulus 'B0' can also defined by Equation (17), [33].

$$B0 = V\frac{\partial^2 E}{\partial V^2} = \frac{4}{9a}\frac{\partial^2 E}{\partial a^2} \quad (17)$$

The unit cell volume 'V' is calculated simply by V = abc for orthorhombic and V = a^2c for tetragonal structures, where a, b, c are lattice parameters [34]. But for a FCC lattice the volume is (1/4) a3 [33], because, four of each atom are present in a unit cell of ZB (FCC) crystal structure, for e.g. for ZnS each Zn atom is surrounded by four equidistant S atoms, at the corners of a regular tetrahedron, similarly each S atom is surrounded tetrahedrally by four Zn atoms. In general, the Murnaghan Equation of state breaks down for compression ratios greater than ~ 0.7 – 0.8 times the original volume, which occurs as a consequence of the triggering nonlinear dependence of the bulk modulus on pressure and variability of bulk modulus pressure derivative at higher pressures. Nevertheless, the bulk modulus is an important physical parameter of crystals; it reflects bonding characters in crystals and, in many instances it is used as an indicator for crystal strength and hardness. A number of researchers have focused upon the bulk modulus in their search for new super–hard materials because the hardness correlates roughly with the bulk modulus for group IV, III–V, and II–VI materials; the bulk modulus results can be extensively used to predict the hardness of a new material [35].

CHAPTER 2 OBJECTIVES

2.1. General Objective

- To Study the structural and electronic properties of a $Be_XZn_{1-X}S$ ternary alloy using ab-initio technique.

2.2. Specific Objective

- To investigate the variations in structural properties of :
  I. Lattice constants, the bulk modulus and pressure derivative.
  II. Electronic properties (band structure and density of states).
  III. The bowing parameters with respect to composition-phase variation on ternary alloy of $Be_XZn_{1-X}S$.
- To Study the effect of Be concentration (X = 0.00, 0.41, 0.66, and 1.00) on $Be_XZn_{1-X}S$ phase transitions.

CHAPTER 3 COMPUTATIONAL FRAMEWORKS

In this chapter, a brief review of the theoretical aspects of our project is presented.

3.1. The Schrödinger Equation

Quantum mechanics gives a logically consistent theory of matter on the microscopic level. It can be considered as the basic theory for many areas of science and technology including solid state physics, atomic physics, particle physics, nuclear physics, chemistry, laser devices and so on. The starting point for any discussion of quantum mechanics is based on the Schrödinger equation [36]. The Schrödinger equation is a differential equation which describes how the wave function Ψ represents a quantum particle's motion under the influence of an external potential V(r). The external potential might be the Coulomb electrostatic potential due to the nuclei of the atoms. The time dependent Schrödinger equation for a quantum particle moving in a three dimensional potential energy field V(r) is given by:

$$i\hbar \frac{\partial}{\partial t}\Psi(r,t) = \hat{H}\Psi(r,t) \tag{18}$$

where, $\hat{H}$ is the Hamiltonian operator which is the sum of a kinetic energy operator and the potential energy of the system. For a single particle of mass m which is moving through space, the Hamiltonian is given by:

$$\hat{H} = -\frac{\hbar^2}{2m}\nabla^2 + V(r) \tag{19}$$

Here, is the reduced, ħ Planck's constant. A fundamental postulate of quantum mechanics states that the possible results of a measurement of an observable represented by the operator Q are its eigenvalues q_i only [37]. The eigenvalue equation is given by:

$$Q\Psi_i = q_i\Psi_i \tag{20}$$

Where Q is an operator and q_i is a number. This is an eigenvalue problem. A solution Ψ of such an equation is called an eigenfunction corresponding to an eigenvalue qi of the operator Q. For the time independent Schrödinger equation, the eigenvalue of the Hamiltonian operator is the energy of the system. For a single particle of mass m which is moving through space, the Schrödinger equation is given by:

$$\widehat{H}\,\Psi = E\Psi \tag{21}$$

3.2. Many Body Systems

Solving the Schrödinger equation for a particular system is important, to understand the behavior of the system, to get information on the density of states of the system, and to understand the response of a particle to an external perturbation [38]. However, the Schrödinger equation has exact solutions for only a few physical problems, such as particle in a box, the simple harmonic oscillator, and the hydrogen atom. For many body systems the Schrödinger equation cannot be solved exactly. Hence, approximation methods are important to solve a many body system's Schrödinger equation. Let us consider a many body system containing N electrons and, in general, several nuclei. We write the full Hamiltonian of this system as:

$$\hat{H} = -\frac{\hbar^2}{2m_e}\sum_i \nabla_i^2 - \sum_{i,I}\frac{Z_I e^2}{r_i} + \frac{1}{2}\sum_{i\neq j}\frac{e^2}{r_{i,j}} - \frac{\hbar^2}{2MI}\sum_I \nabla_I^2 + \sum_{I,J}\frac{Z_I Z_J e^2}{R_{I,J}} \quad (22)$$

Here, $r_{ij}=|r_i-r_j|$, $R_{IJ}=|R_I-R_J|$, and r_{iI} represents the distance from electron (i) to nucleus (I). The five terms in this equation define, sequentially, the kinetic energy of all the electrons with mass m_e, the interaction potential energy between all electrons and the atomic nuclei, the interaction energy between different electrons, the kinetic energy of all the nuclei with mass MI, and finally the interaction between the nuclei. Because of the presence of the electron-electron interaction term in the Hamiltonian in equation (22), the Schrödinger equation is not separable. Therefore, approximation methods must be used to solve the many body Schrödinger equation [36]. The separation of nuclear motion and electronic motion into two mathematical problems is called the Born-Oppenheimer approximation [39]. This approximation method assumes that the motion of the nuclei is so much slower than the motion of the electrons and can be considered to be stationary. The Born-Oppenheimer approximation allows us to neglect the kinetic energy term of the nuclei in the Hamiltonian, and the electrostatic repulsion between positively charged nuclei simply represents a constant in the electronic problem. The electronic "clamp-nucleus" Hamiltonian can now be written as:

$$\hat{H} = -\frac{\hbar^2}{2m_e}\sum_i \nabla_i^2 - \sum_{i,I}\frac{Z_I e^2}{r_i} + \frac{1}{2}\sum_{i\neq j}\frac{e^2}{r_{i,j}} + \sum_{I,J}\frac{Z_I Z_J e^2}{R_{I,J}} \quad (23)$$

where, the last term is the nucleus-nucleus interaction, which has a constant value. Still the present version of the Schrodinger equation is too complex to be solved due to the electron - electron interaction term.

3.3. The Hartree-Fock Approximation

The Hartree-Fock approximation is a natural starting point of quantum mechanical calculations for many body systems. The theory approximates the wave function of the many body systems in terms of products of single electron wave function. In this method the total Hamiltonian $\widehat{H}$ is sum of single electron Hamiltonian operators $\widehat{H}i$. The functional form of the many electron system wave function can be expressed in terms of a single product of single electron wave functions,

$$\Psi(r_1, r_2 \ldots r_N) = x_{1(r_1)} x_{2(r_2)}, \ldots x_{N(r_N)} \tag{24}$$

These single electron wave functions are called spin orbitals. Each spin orbital is a product of a special function and a spin state (up and down). This form of Ψ is known as a Hartree product. The Hartree product of spin orbitals has a serious drawback [39]. It does not satisfy the antisymmetry principle, a main criterion for a many fermions wave function. According to quantum mechanics, electrons are fermions, and the antisymmetric principle states that if two electrons are interchanged, the wave function must change sign:

$$\Psi(r_1, r_2) = -\Psi(r_2, r_1) \tag{25}$$

The most convenient way to write the wave function of a many electron system is in terms of a Slater determinant of single electron wave functions [39]. The inclusion of a Slater determinant representation of the many electron system into the Hartree theory gives the Hartree-Fock theory. In a Hartree-Fock calculation, the Coulomb electron-electron interaction potential can be written as:

$$V_{H(r)=e^2 \int \frac{n(r)}{[r-r']} d^3r} \tag{26}$$

The Hamiltonian $\hat{H}$ corresponding to each electron therefore has a form:

$$\hat{H} = T + V + V_H \tag{27}$$

Where V_H (r) is the Hartree potential or mean field potential. This is an average Coulomb interaction potential between a single electron and the rest of the electrons in the system.

For the N electrons and with spin orbitals, the Slater determinant can be written as:

$$\Psi(x_1, x_2, \ldots, x_N) = \frac{1}{\sqrt{N!}} \begin{vmatrix} \chi_1(x_1) & \chi_2(x_1) & \cdots & \chi_N(x_1) \\ \chi_1(x_2) & \chi_2(x_2) & \cdots & \chi_N(x_2) \\ \vdots & \vdots & \ddots & \vdots \\ \chi_1(x_N) & \chi_2(x_N) & \cdots & \chi_N(x_N) \end{vmatrix} \equiv |\chi_1 \ \chi_2 \ \cdots \ \chi_N|, \tag{28}$$

Here, $\frac{1}{\sqrt{N!}}$ is normalization factor. The Slater determinant fulfills the Pauli Exclusion Principle. Exchanging any two rows of a determinant changes the sign of Ψ, which leads to the anti-symmetry principle. If any two rows of a determinant are identical, the determinant will vanish. No two identical electrons occupy the same spin orbitals simultaneously. The Hartree- Fock method gives an exact account of electron exchange [39].

3.4. Density Functional Theory

In the Hartree-Fock theory, the N electron wave function can be approximated using a single Slater determinant. The central idea behind density functional theory (DFT) is to use the electron density as a basic variable, instead of using the many-electron wave function. Density functional theory can be traced back to the works of Thomas and Fermi in the 1920s [40, 41]. The entire field of density functional theory rests upon the two fundamental mathematical theorems proved by Hohenberg and Kohn in 1964 and the Kohn-Sham formulation of density functional theory in 1965 [42].

3.5. The Hohenberg-Kohn Theorems

The starting point of any discussion of DFT is the Hohenberg-Kohn theorems [43]. The first theorem states that for any system of interacting particles in an external potential, the ground state electron density, n (r), determines the external potential Vext (r) fully and uniquely. In other words, there exists a one to one relationship between the electron density and the external potential,

$$n(r) \rightarrow V_{ext(r)} \tag{29}$$

According to this theorem, the total energy functional E [n (r)] is expressed as:

$$E[n(r)] = \int V_{ext(r)n(r)dr} + F_{HK}[n(r)] \tag{30}$$

where Vext (r) is an external potential (mainly from the nuclei). F_{HK} [n(r)] is known as a universal functional, because it does not depend on the external potential. It is the sum of the

kinetic energy of the electrons and the contribution from inter electronic interactions. It is given by:

$$F_{HK}[n(r)] = T[n(r)] + \frac{1}{2}\sum V_H\,[n(r)]n(r)dr \qquad (31)$$

The second Hohenberg-Kohn theorem shows that if n (r) is normalized to the number of Particles in the system, then the total energy of the system E [n (r)] becomes a minimum if and only if n (r) is the exact ground state density.

3.6. The Kohn-Sham equations

The Hohenberg-Kohn theorems state that the ground state density uniquely determines all ground state observables and it can be determined from the ground state energy functional E [n (r)]. However, the theorem does not give us a hint about how to solve the full Schrödinger equation. For example, there is no exact expression for the electron exchange-correlation functional which includes all quantum mechanical effects. These problems were addressed by Kohn and Sham in 1965 [44]. In the Kohn-Sham scheme, the ground state electron density can be expressed by a set of equations which only involves a system of non-interacting electrons. This non-interacting system has the same electron density n (r) as the original system. The energy functional for this system can be given by:

$$E[n(r)] = T_s[n(r)] + \int V_{eff(r)n(r)d^3r} \qquad (32)$$

The Kohn-Sham equations for electrons moving in an effective external potential can be written as:

$$\left[-\frac{\hbar^2}{2me}\nabla^2 + V_{KS}(r)\right]\varphi_i(r) = \varepsilon_i\varphi_i(r) \tag{33}$$

The solution to this Schrödinger equation yields the Kohn-Sham eigenvalues. The kinetic energy of a system of non-interacting electrons with density n (**r**) is given by:

$$T_{S[n(r)]} = \sum i \left\langle \varphi_i \middle| -\frac{\nabla^2}{2} \middle| \varphi_i \right\rangle \tag{34}$$

where the density of the interacting system is determined by:

$$n_{S(r)=\sum_i|\varphi(r)|}2 \tag{35}$$

The effective external potential is given by:

$$V_{KS(r)=}V_{ext(r)} + V_H(r) + V_{XC}(r) \tag{36}$$

Here, Vext (r) is the Coulomb interaction between an electron and the atomic nuclei, V_H (r) is the classical (Hartree) potential describing the Coulomb interaction between the electrons, and V_{XC} (r) is the exchange and correlation potential, which describes all the quantum mechanical effects.

The exchange and correlation potential can be formally defined as a functional derivative of the exchange-correlation energy with respect to the electron density,

$$V_{XC}(r) = \frac{\delta E_{XC[n(r)]}}{\delta n(r)} \tag{37}$$

3.7. The Exchange-Correlation functional

The major problem in solving the Kohn-Sham equations is that the true form of the exchange correlation functional is not known. The local density approximation (LDA) is the first approach to approximate the exchange-correlation functional in DFT calculations. In this approximation, the local exchange-correlation potential at each position r is the exchange correlation potential for a homogeneous electron gas at the electron density observed at that position [19].

$$V_{XC}{}^{LDA}[n(r)] = \int \rho(r)\, \varepsilon_{xc}\big(\rho(r)\big)dr \tag{38}$$

The LDA approximation is exact for a homogeneous electron gas, but the real electron densities are not typically homogeneous over the entire system. The second well known class of approximations to the Kohn-Sham exchange-correlation functional is the generalized gradient approximation (GGA). In the GGA approximation the exchange and correlation energies include the local electron density and the local gradient in the electron density [39],

$$V_{XC}{}^{GGA}[n(r)] = \int \rho(r)\, \varepsilon_{xc}(\rho(r)\nabla(\rho(r))dr \tag{39}$$

3.8. Solving the Kohn-Sham equations

Once we have approximated the exchange-correlation energy, we are in a position to solve the Kohn-Sham equations. The Kohn-Sham equations have an iterative solution; they have to be solved self-consistently. To solve the Kohn-Sham equations for a many body system, we need to define the Hartree potential and the exchange-correlation potential. To define the Hartree potential and the exchange-correlation potential, we need to know the electron density n(r). However, to find the electron density, we must know the single electron wave functions. We do

not know these wave functions until we solve the Kohn-Sham equations. The well known approach to solve the Kohn-Sham equations is to start with an initial trial electron density as illustrated in Figure (3). Then solve these equations using the trial electron density. After solving the Kohn-Sham equations, we will have a set of single electron wave functions. Using these wave functions, we can calculate the new electron density. The new electron density is an input for the next cycle.

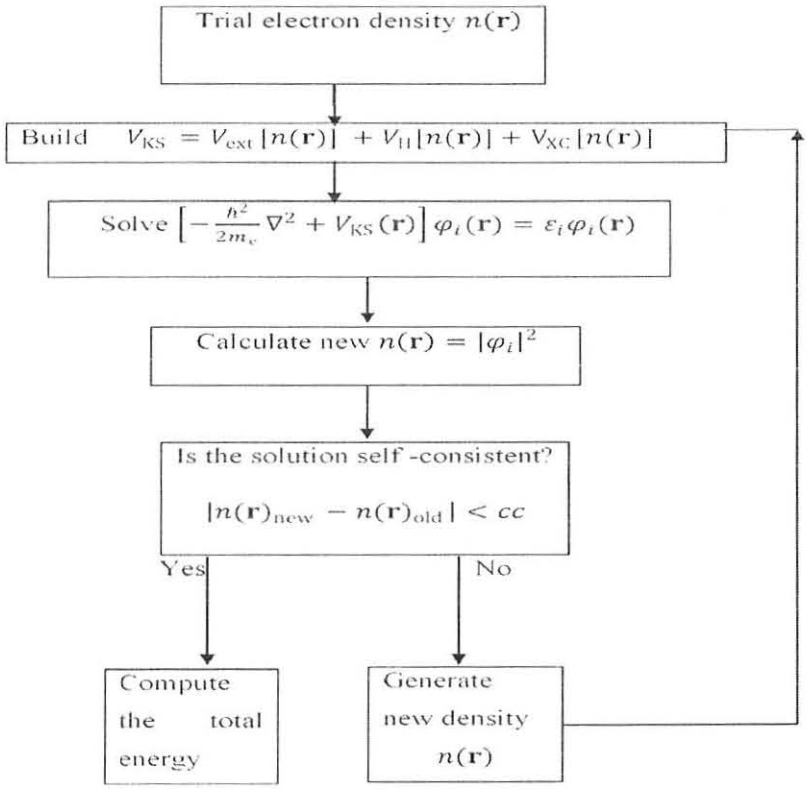

Figure 3. Illustration of the self-consistent field (SCF) procedure for solving the Kohn-sham equations where cc is an appropriately chosen convergence criterion

Finally, compare the difference between the calculated electron densities for consecutive iterations. If the difference in electron density between consecutive iterations is lower than an

appropriately chosen convergence criterion, then the solution of the Kohn-Sham equations is said to be self-consistent. Now the calculated electron density is considered as the ground state electron density, and it can be used to calculate the total energy of the system [39].

CHAPTER 4 METHODOLOGY FOR ATOMISTIC SIMULATIONS

4.1 Software used for computation

The computational tools that are used to carry out the theoretical analysis are TRANSIESTA based Atomistic Toolkit software implementation code for performing electronic structure calculations. Python as a script language and Atomistic Tool Kit (ATK) is a versatile software platform for atomistic simulations of nanoscale systems.

4.2. TRANSIESTA

SIESTA (Spanish initiative for electronic simulations with thousands of atoms) [47] is a method and a software implementation for performing electronic structure calculation and ab initio molecular dynamics simulations of molecules and solids. It uses a DFT code that predicts the physical properties of a collection of atoms. Properties that can be predicted using the code includes the Kohn-Sham band structures, electrons density, and Mullikan populations. Modern SIESTA code used for the study of transport properties is termed as TRANSIESTA.

4.3. Python language and virtual nanoLab

Python is an interpreted language, which can save you considerable time during program development because no compilation and linking are necessary. The interpreter can be used interactively, which makes it easy to experiment with features of the language [48]. Python allows writing very compact and readable programs. A software platform for atomistic simulations of nanoscale systems has the following parts:

- **Atomistix Toolkit** (ATK)

- State-of-the-art DFT engine for electronic structure and transport calculations.

➢ **Virtual NanoLab** (VNL)

- Modern graphic user interface GUI for setup and analysis.

➢ **NanoLanguage**

- Scripting language interface to ATK.
- Fully integrated in VNL.

The strength of ATK and VNL lies in their flexibility to describe systems of different symmetries. It can describe isolated systems (molecules), periodic systems (crystals), and system of the type bulk-nanodevice-bulk (two probe systems). Atomistic Toolkits (ATK) gives you access to a powerful set of modeling tools for investigating a variety of nanoscale systems such as molecules, bulk, and two-probe systems. The systems may contain nanowires, nanotubes, graphene, semiconductors, metals, etc

4.4. Simulation methods and samples preparation

In this section, we first constructed a model of the atomic configuration to our investigation. The idea of this constructing an alloy by taking a unit cell (cubic two atoms) and repeating it three dimensionally for the calculation of the electronic structure of the semiconductor alloy has been used for the binaries. The full structure optimization of cell parameters and internal coordinates is performed in all super cells prior to calculations of electronic, structural, DOS, and effect of pressure. Bulk $Be_XZn_{1-X}S$ ternary alloy have studied in this work is modeled by repeating 3 x 3 x 3 FCC super cell conformation with 54 atoms per super cell since 2 x 3^3 = 54, two atoms per unit cell. These is done using bulk builder from the SIESTA software, at Be concentration (X) of 0, 0.41, 0.66, and 1, completely the full range of alloying is replicated and infinitely enlarge the

system by repeating such a super cell. In the zinc blende-like structure, the atoms are tetrahedrally bonded so that each S atom is surrounded by four cations (Be or Zn). In the same manner also the rock salt modeling is the same but the difference among from the zinc blende modeling is the atomic position. S (sulfur) is slightly changes from (0.25, 0.25, and 0.25) to (0.5, 0.5, and 0.5). In both cases (ZB and RS) the position of the Be is the same. After modeling the sample using its standard atomic structure we drop it to the NanoLanguage Scripter (NLS) and thus creating complete calculation script by using appropriate geometric optimization parameters and set-ups then we store this as NanoLanguage script and finally we execute (run) the scripts using the ATK computation engine and standard command syntaxes. This would give us the configurationally optimized samples for different concentrations. The resulting sample geometric xyz files are saved as python (.py) extension. It is to be noted that for the concentrations (X) of 0.41 and 0.66 we have replaced eleven and eighteen Zn atoms from ZnS, respectively, by Be atoms to get the desired concentrations. For the calculation of the structural properties, the crystal structures are optimized by force minimization (Quasi Newton method) in which the atoms are allowed to move towards the equilibrium positions. The different optimized simulation samples prepared for $Be_XZn_{1-X}S$ ternary alloy have shown in three dimensions, Figure (4).

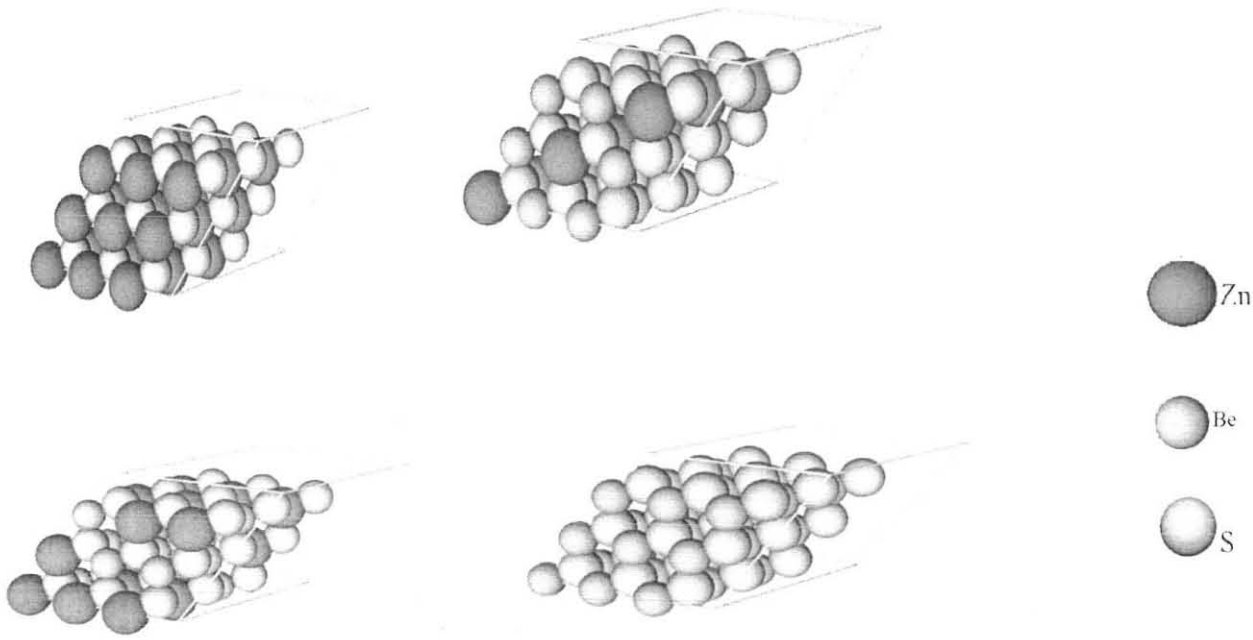

Figure 4. The schematic diagram of optimized structures of a $Be_XZn_{1-X}S$ alloy at Be concentration (X) of a) 0.00 b) 0.41 c) 0.66 and d) 1.00

In order to carry out the study of structural and electronic properties of the samples, we have performed the following sets of simulation experiments, Total energy (E_T), band structures (BS), density of states (DOS), etc. with the help of the following basic procedures performed by the above sets of experiments. First, we take crystal of ZnS from the crystal board and put on the bulk builder then, prepare python script at different lattice constant for the seek of further calculation Second step, take the prepared python script on the NLS for the seek of defining the physical properties such as configuration(geometric optimizations), method, and analysis.

a) ZnS

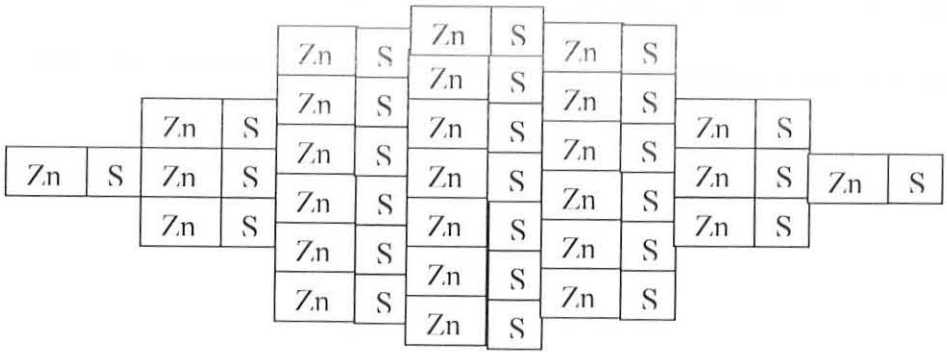

b) $Be_{0.41}Zn_{0.59}S$

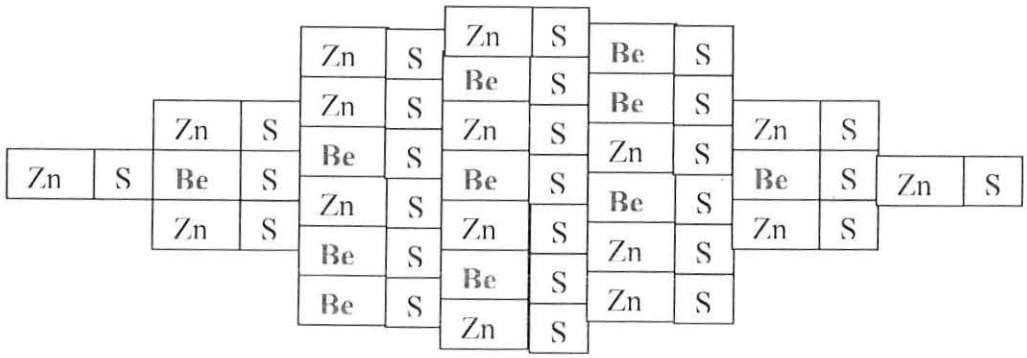

c) $Be_{0.66}Zn_{0.34}S$

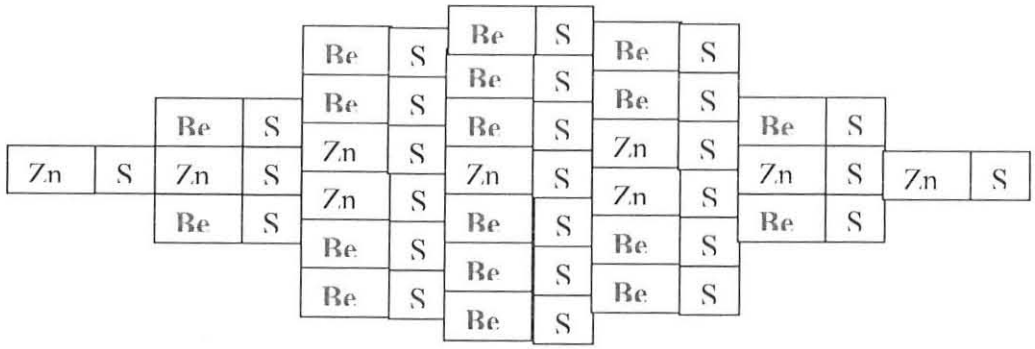

d) BeS

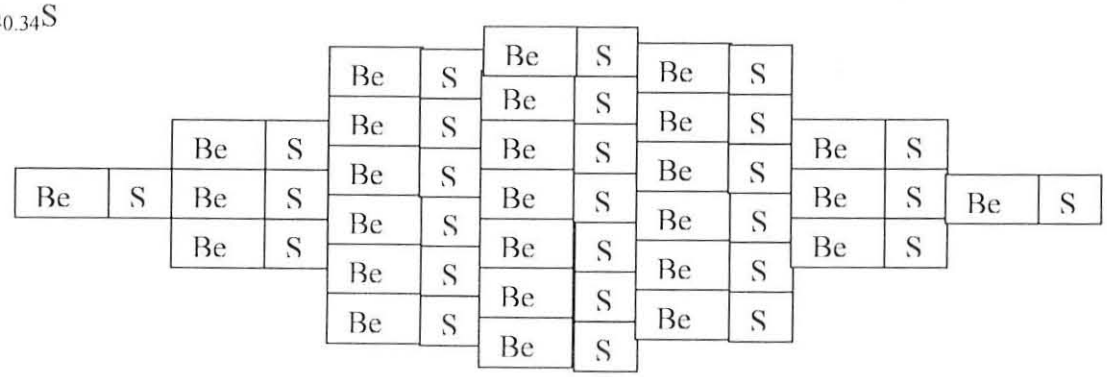

Figure 5. The schematic diagram of optimized structures of a $Be_XZn_{1-X}S$ alloy at Be composition (x) of a) 0.00 b) 0.41 c) 0.66 and d) 1.00 in to 2D with position of dopant.

Table 1. Basic parameters used for our calculations for the ab-initio alloy modeling.

parameters	Bulk system	Values
Basis set	Type	Double zeta polarized
	Energy shift	0.01 Rydberg
	Delta rinn	0.8
	Vo	40 Rydberg
	Radial sampling DR	0.001 Bohr
Brilliouin Zone integration	Number of K-points (A)	5
	Number of K-points (B)	5
	Number of K-points (C)	5
Eigen state occupation	Left and right electrode electron temperature	300 Kelvin
Electron density	Mesh Cut-off	150 Rydberg
Exchange Correlation Functional	LDA-PW	
Iteration control	Tolerance	$1x10^{-5}$
	Criterion	Total energy
	Max steps	200
Iteration mixing	Quantity	Hamiltonian
	Diagonal mixing parameter	0.1
	History steps	6

Table 2. The VNL toolbar, which provides access to different stages of sample or device preparation and characterization.

Tools	Icon	Description
Crystal Cupboard		Database of bulk crystals
Atomic Manipulator		Set up two-probe systems and make modifications to two probe device
Molecular Builder		Build and construct your own molecules ready to be used in other VNL tools
NanoLanguage Scripter .		Create complete calculation set-ups and store these as Nano-Language script
Script Editor	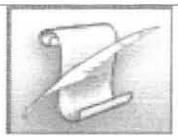	Manually edit and NanoLanguage scripts constructed by the different set of VNL tools.
Job Manager		Execute scripts using the ATK computation engine.
Nanoscope		Visualize atomic geometries and calculated properties in 3D.
Result Browser		Browse the contents of VNL files including all stored samples and results within them.

Finally the numerical calculation file (.nc) is created under the self-consistent tab. Under analysis tab of NLS we defined different quantities. As the program execution terminated normally, a complete calculation file is obtained from the log window and is stored for the further analysis.

CHAPTER 5 RESULTS AND DISCUSSION

In this part, the results of our calculations are presented. First, structural and electronic properties (band gap and DOS) of ZnS, BeS zinc blendes and, the effects of incorporation of Be substitution on the super cell of ZnS at (X = 0, 0.41, 0.66) and X = 1.00 compositionally valued on the structural and electronic structure are presented. Secondly, structural and electronic properties (band gap and DOS) of ZnS and BeS in the rock salt form and the effects of incorporation of Be substitution on the super cell of ZnS at (X = 0, 0.41, 0.66) and X = 1.00 compositionally valued on the structural and electronic structure are presented. Finally, the effect of high pressure on $Be_XZn_{1-X}S$ alloys at (X = 0, 0.41, 0.66 and 1.00), phase transition from ZB→RS.

5.1. Structural Properties for $Be_XZn_{1-X}S$ Alloys in Zinc blende and Rock Salt Structure

The structural properties of ZnS, BeS compounds and their ternary alloys in the zinc blende and rock salt phase using the LDA. For the considered structures and at different beryllium concentrations (X = 0, 0.41, 0.66, 1), the structural properties were obtained by a minimization of total energy as a function of the volume for ZnS, BeS and $Be_XZn_{1-X}S$ in the ZB and RS structures. This allowed the obtaining of the equilibrium structural properties, the lattice constant (a), the bulk modulus (B0) is fitted by Murnaghan's equation of state [4]. The equilibrium lattice constants and bulk modulus for the binary compounds (ZnS and BeS) and their alloy ($Be_XZn_{1-X}S$) are given in Table 3 and Table 4, for ZB and RS, respectively, which also contain results of previous calculations as well as experimental result.

Table 3. Lattice constants a_{eq} (Å) total energy (eV) and bulk modulus B0 for ZB structure of ZnS, BeS and $Be_XZn_{1-X}S$ alloys.

X	Values	a_{eq}(Å)	E_T (eV)	B0 (GPa)	P_T (GPa)
0	This work	5.31	-52381.3205	63.8	20.0
	Exp't	5.41 [22]	-	76.9 [22]	18.1, 16.2 [50]
	Other calc	5.46, 5.53, [22]	-	80.6, 69.4, 69.6 [22], 83.1 [29]	16.1 [50] 4.9 [29]
1	This work	4.81	-10687.2826	96.0	61.0
	Exp't	4.87, 4.86 [51, 11]	-	105.0 [10]	51.8 [11]
	Other calc	4.82	-	93.0 [10] , 92.2 [49]	49.9 [11]
0.41	This work	5.13	-35389.7507	70.3	32.6
0.66	This work	5.08	-24579.6819	90.1	26.0

Table 4. Lattice constants a (Å) total energy (eV) and bulk modulus B0 for RS ZnS, BeS and $Be_XZn_{1-X}S$ alloys.

X	Values	a_{eq}(Å)	E_T (eV)	B0 (GPa)
0	This work	4.99	-52372.1469	90.2
	Exp't	5.06 [49]	-	103.6 [49]
	Other calc	5.21 [49]	-	83.1 [49] ,104.4 [29]
1	This work	4.54	-10664.3363	130.9
	Exp't	4.88	-	
	Other calc		-	
0.41	This work	4.86	-35377.9223	110.0
0.66	This work	4.69	-24564.3414	119.9

The total energy determined here in Table 3 and Table 4 shows the robustness and the stability of the modeled alloy materials for the calculations of the ground state properties. It should be noted that, there is no available experimental or theoretical publication of these values for the alloys of 0.41 and 0.66 to be compared with. Nevertheless, our results for the binary compounds are reasonable with experimental investigations. However, we have a small under estimation of the lattice parameters and bulk modulus when we compare our results to the experimental data. This may possibly due to the use of the LDA. The LDA is the ground state theory, which cannot do very well in the excited state. In both cases (ZB and RS) our calculated values of the lattice constants for the binary compounds are slightly underestimated compared to the corresponding experimental values, which is consistent with the general trend of the LDA approximation. This shows that our calculations underestimate the equilibrium lattice parameter by 1.31 - 1.77% and

bulk modulus (B0) by 5 - 13% with respect to experimental data. Nevertheless, our calculated structural parameters are in good agreement with those obtained by first principles methods within different approximations. Generally speaking, the lattice parameters that we have estimated from the Vegard's expression (Equation 1) are comparable with the DFT calculation for the respective concentrations. Figure 6 (a) and (b); show the variation of the calculated equilibrium lattice constant *versus* concentration (X) for $Be_XZn_{1-X}S$ alloy for ZB and RS respectively. We found that the configurationally averaged lattice constants from Vegard's law have only a small deviation, which are illustrated by dotted curve as a linear variation of the lattice constant of alloys *versus* concentration (X). However, from the literature survey it is turned out that the violation of Vegard's law has been reported in semiconductor alloys both experimentally and theoretically [4]. Usually, in the treatment of alloys, it is assumed that the atoms are located at the ideal lattice sites and the lattice constant varies linearly with concentration X according to the so-called Vegard's law. Our results for all compounds are comparable with the reported theoretical investigations. A small deviation from Vegard's law (the lattice constant of alloys should be linearly with concentration (X) is found for this alloy with upward bowing parameter equal -0.269 Å and -0.097 Å obtained by fitting the calculated values with a polynomial function for ZB and RS, respectively. The result of the RS is in good agreement with the theoretical values of (-0.066 Å) and (-0.016 Å) [4]. But the ZB values are more deviated from the theoretical one.

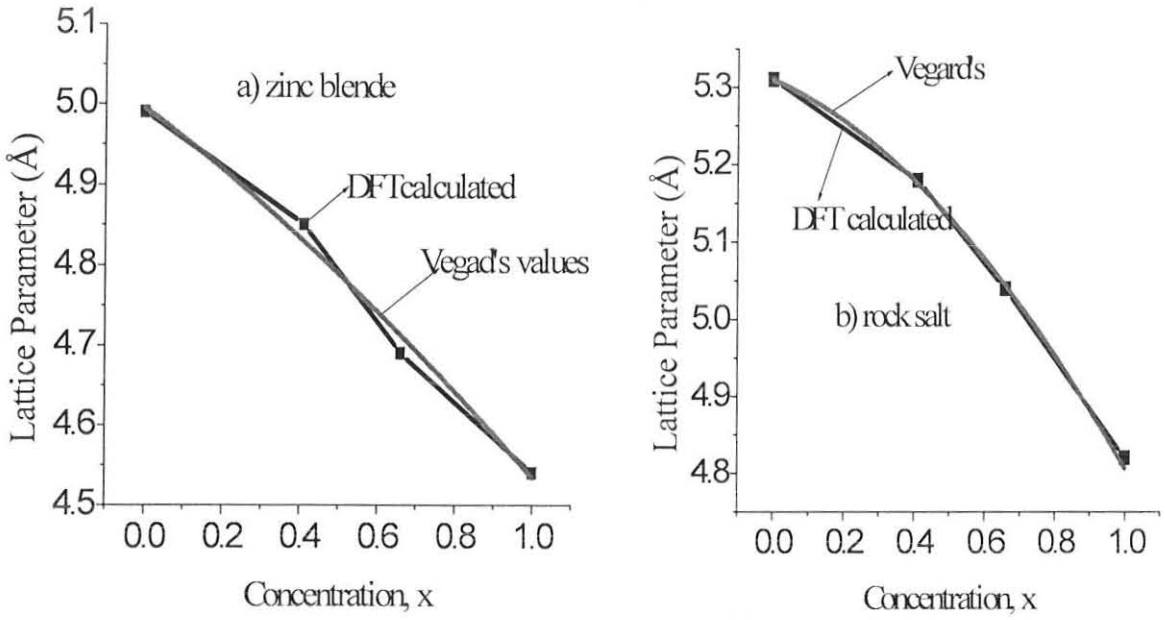

Figure 6. Shows the variation of the calculated equilibrium lattice constant *versus* concentration for $Be_XZn_{1-X}S$ alloy at different concentration of beryllium (X = 0, 0.41, 0.66, 1.00) in the form of a) ZB b) RS.

The physical origin of this deviation should be mainly due to the large mismatches of the lattice constants of the binary compounds ZnS and BeS [4]. The Vegard estimates show that the substitution of Zn by Be accompanied with monotonic decrease of the lattice parameter [52]. Similarly our calculated lattice constant of a $Be_XZn_{1-X}S$ alloy in both cases (ZB and RS) decreases linearly with increasing X value according to Vegard's rule. However, our DFT calculated lattice constant *versus* concentration curve shows a slight increases of the lattice constant at X value of 0.41 and decreases at X value of 0.66 Figure (6) as compared with Vegard's law. As we observed from Figure (7), shows the variation of the calculated bulk modulus *versus* concentration 'X' for a $Be_XZn_{1-X}S$ alloy are calculated and there is a linear deviation of bulk modulus from the vegard's of average configuration. This deviation is due to

the weak mismatches of the bulk modulus of the binary compounds. Note that as the concentration (X) increases, B0 increases as well. The enhancement of B0 *versus* (X) is monotonic. This indicates that the material under load becomes less compressible when increasing the alloy concentration (X) [4]. A marginal deviation from LCD, with downward bowing equal to -4.486 Gpa and 1.050 Gpa for the ZB and RS, respectively was observed. In the same manner the increments of bulk modulus is due to the more covalence character of BeS.

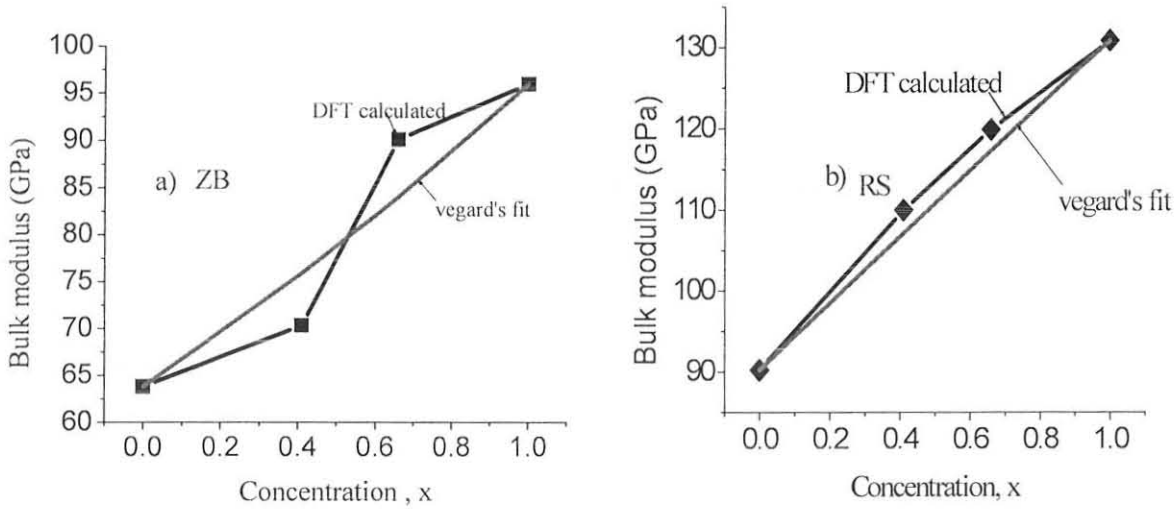

Figure 7. Concentration dependence of the DFT calculated bulk modulus of a BeXZn1-XS alloy compared with the linear concentration dependence prediction as estimated from the vegard like average configuration.

Our DFT calculated bulk modulus *verses* concentration curve shows the general trend of increase in the bulk modulus with increase in Be concentration. As shown in Figure 7 a slight decrease and increase of the bulk modulus at X = 0.41 and 0.66, respectively, is clearly visible as compared to the linear concentration dependence, that is a dotted curve in Figure 7 (a). The reason for these anomalies can be explained as follows. The bulk modulus of the material has an

inverse relation with bond length and at X = 0.41, ZnS have large bond concentrations than BeS bond. Therefore, BeS has less effect on bulk modulus due to lower bond concentrations, but ZnS shows 1-bond → 2-mode behaviour, which implies that one ZnS bond, has larger value than its equilibrium value, hence bulk modulus decreases. Similarly at X = 0.66 BeS has more bond concentration and shows 1-bond → 2-mode behaviour i.e. 1-mode of BeS should have smaller bond length in comparison to its equilibrium bond length, hence increase in the bulk modulus. But in case of Figure 7 (b), generally the bulk modulus increase slightly through our calculation at all selected concentrations of our materials. The reason is that the effect of pressure can bring that decreasing the lattice constant of the materials meaning decreasing the bond length of alloys but increases the bond concentration at the X = 0.41 and 0.66 and has more bond concentration and shows 1-bond → 2-mode. Generally, our DFT calculated parameters of ground state moduli are in good agreement to experiments and other reported theoretical investigations, which give us much promised to investigate the other properties of the alloy under pressure.

5.2. Pressure effect on structural properties of $Be_XZn_{1-X}S$ alloys

In the $Be_XZn_{1-X}S$ system, the constituent components ZnS, BeS and $Be_XZn_{1-X}S$ alloys exhibit contrasting properties, and their pressure-induced phase transformation also follows different paths. Pure ZnS and BeS both crystallize in the zinc blende (ZB) structure at low pressure and are known to transform to cubic rock salt (NaCl) at high pressure. The phase transformation pressure increases linearly with Be concentration (X) [53]. In this work we computed the structural properties of $Be_XZn_{1-X}S$ alloys at high pressure by using the first-principle ab-initio SIESTA methods. Under this condition, the information needed to determine the transition pressure is the total energy variation with volume and pressure *versus* volume relation. The structure of $Be_XZn_{1-X}S$ alloys phase is optimized at the pressure of zero (0) GPa. The calculated

energy volume data of the ZB and RS structures of $Be_XZn_{1-X}S$ alloys are shown in Table 3 and 4 respectively. Our calculation for $Be_XZn_{1-X}S$ follows the transformation sequence of ZB to RS, which agrees with the recently reported theoretical as well as experimental investigations at X = 0 and 1. Our results show that a first-order phase transition from the ZB structure to the dense RS structure is at approximately 20.0 GPa and 61.0 GPa respectively. For the case of X = 0.41 and X = 0.66 the calculated phase transition pressure is 32.6 Gpa and 57.0 Gpa respectively.

As shown from Figure 8, the pressure phase transition is observed. Thus transition pressures are calculated from the pressure –volume data that is calculated from the E-V data.

a)

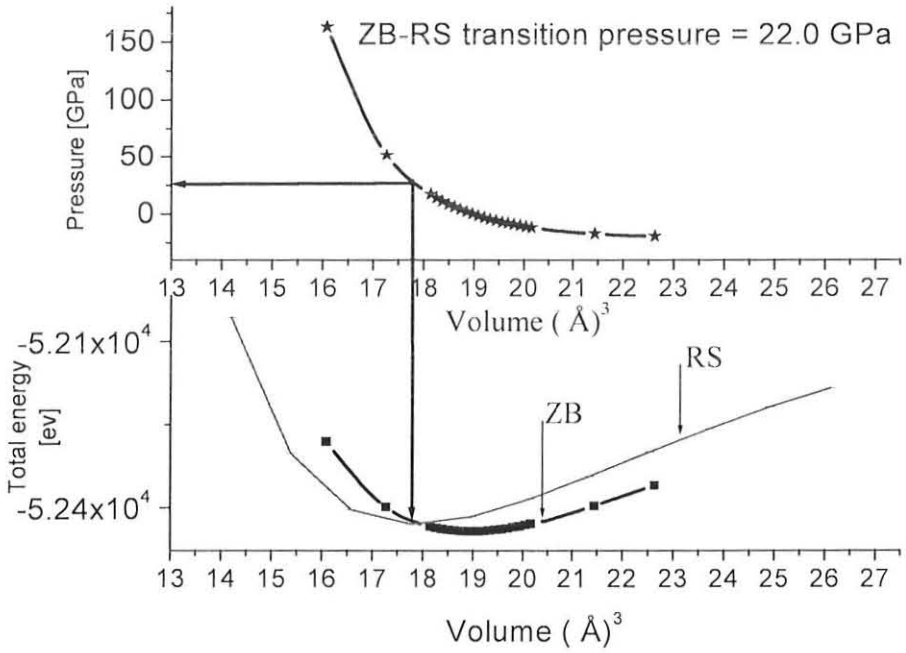

b)

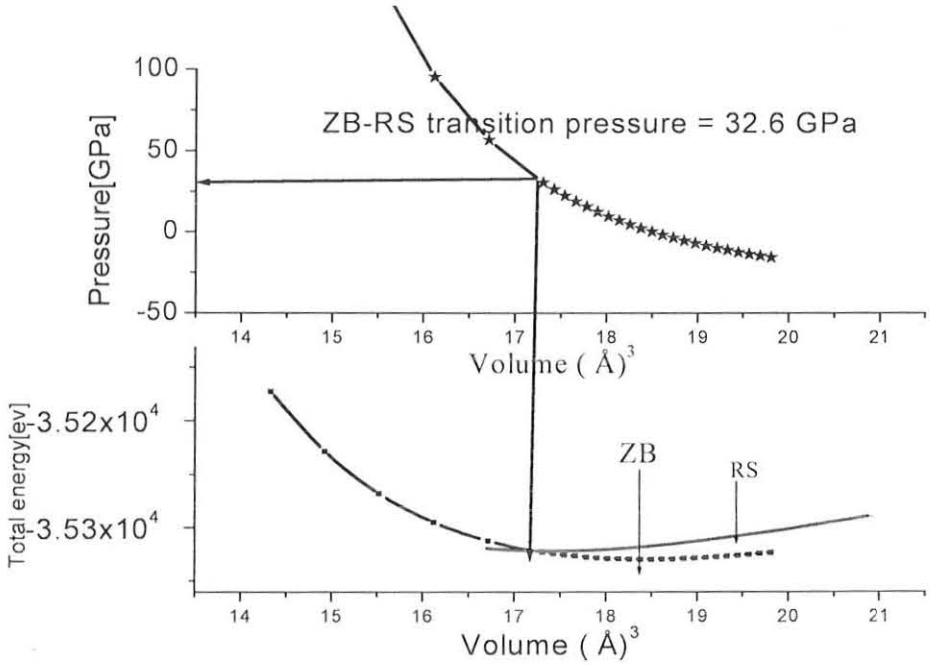
ZB-RS transition pressure = 32.6 GPa
Pressure[GPa]
100
50
0
-50
14
15
16
17
18
19
20
21
Volume (Å)3
Total energy[ev]
-3.52x10^4
-3.53x10^4
ZB
RS
Volume (Å)3

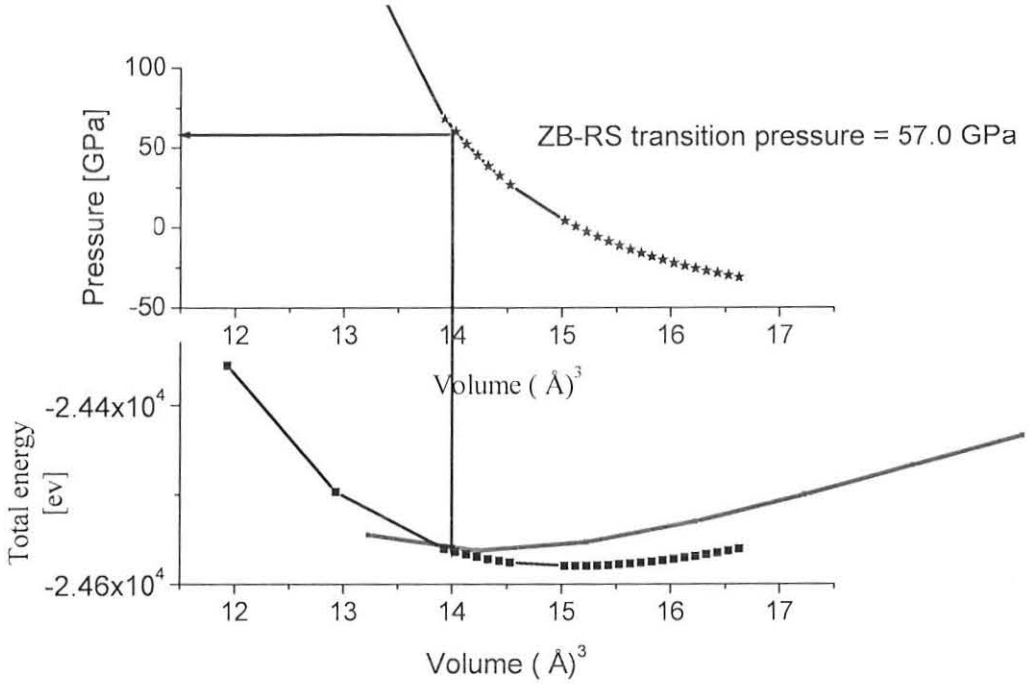
ZB-RS transition pressure = 57.0 GPa
Pressure [GPa]
100
50
0
-50
12
13
14
15
16
17
Volume (Å)3
Total energy [ev]
-2.44x10^4
-2.46x10^4
Volume (Å)3

c)

d)

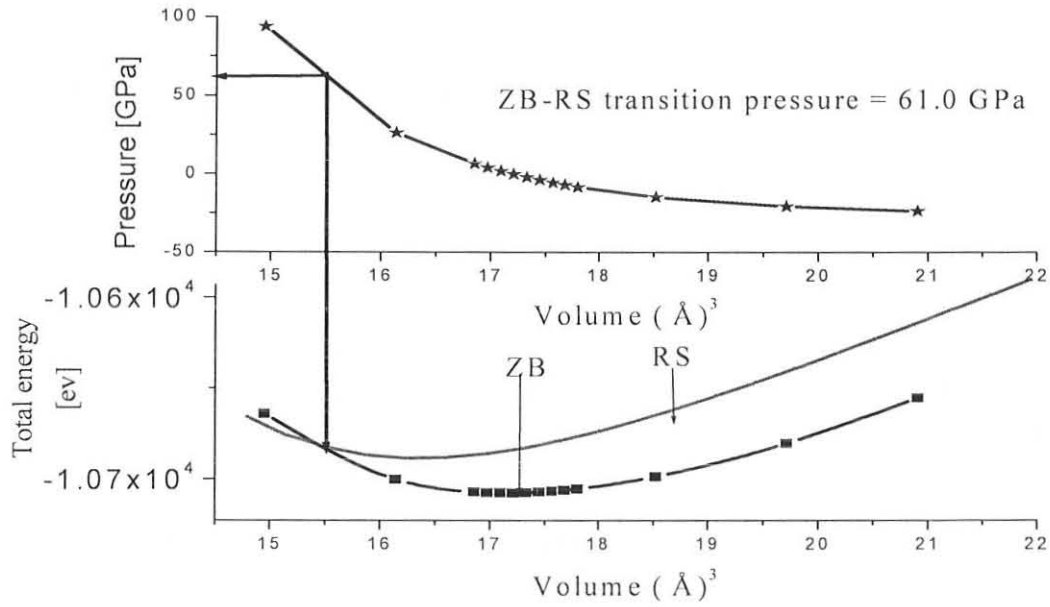

Figure 8. The phase transition of ZB to RS at concentration of Be a) 0.00 b) 0.41 c) 0.66 and d) 1.00 with pressure - volume data.

The obtained values of a_{eq}, B0, E_T, and transition pressure (P_T) of ZB to RS phase of ZnS and BeS compared with some available theoretical studies and our calculated ZB to RS transformation pressure is slightly above experiment but is in good agreement with an theoretical data of [11, 50]. For the selected concentration of Be atoms, at X = 0.41 and X = 0.66 the phase transition pressure is 32.6 Gpa and 57 Gpa respectively. This shows, as the Be atom substitutions increases phase transition pressure increases. This indicates that the effect of Be atoms have the tendency it required high pressure to change the phase of the alloys. The obtained results show ZB structure is more stable than RS structure. That is, the energy state of ZB structure is the lower as compared to the RS structure, which is clearly visible in Table 3 and 4, as the lower energy minima corresponding to ZB phase. In addition, our calculated bulk modulus of RS

structure is much higher than that of ZB structure. The materials are more closed packed volume decreases relative to the less packed one (ZB). This is because high pressures applied will forces the atoms closer to each other with decreasing inter-atomic spacing between the atoms in the lattice. Consequently the bond exhibit the covalency nature, thus have larger bulk modulus. Moreover, the elastic constant of the materials at high pressures is essential in order to predict and understand the material's response, strength, mechanical stability, and phase transitions.

5.3. Band Structure for zinc blende crystal structure

The band gap is the minimum energy of an electronic excitation in which there is no interaction between the promoted electron and the hole that it leaves behind. In terms of the Kohn-Sham description of the system, the band gap is usually taken to be the difference between the eigenvalues of the conduction band minimum and the valence band maximum, which are the bands positioned at just first two points on the either side of the zero point (E_F). The calculated electronic band structure shows zinc blende ZnS is a direct band gap material with the top of the valence band and the bottom of the conduction band occurring at the zone center of Γ. This indicates that there is no momentum change. The calculated fundamental band gap or energy difference between the top of the valence band and the bottom of conduction band is depicted in tables 5. The calculated band gap is underestimated in comparison with the experimental result, but the overall electronic band profiles are very comparatively in good agreement with the theoretical values.

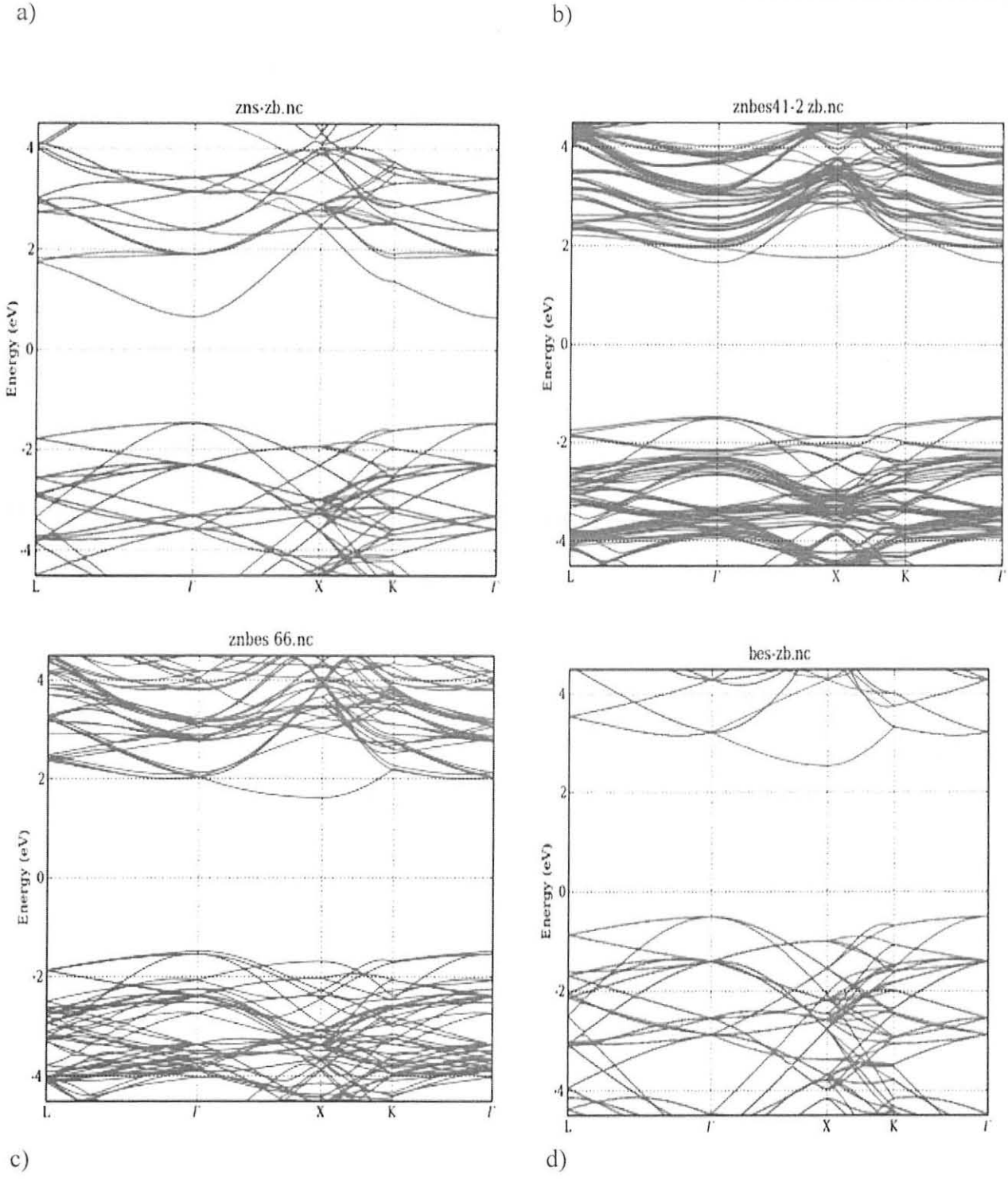

Figure 9. Band structures of a $Be_xZn_{1-x}S$ alloy at Be concentrations (x) of a) 0.00 b) 0.41 c) 0.66 and d) 1.00.

As we see from the Figure 9 (b) still the band gap is a direct as the 0.41 incorporation of Be atoms in to the super cells. We note that the fundamental gap (Γ–Γ) increases from Figure 9 (a) to Figure 9 (d) almost linearly with increase of the Be concentration. This is because an increasing replacement of Zn atoms by Be causes the atoms closer to each other (the smaller the volume per atom), the stronger character of the covalent bonds is observed. Thus due to the covalent character of Be, the cations state exhibit less orbital overlap extent and thus more sharing of electrons, which leads to the increasing of the energy bands (valence band and conduction band). In Figure 9 (c) the calculated electronic band structure is allowed the indirect band gap as the Be concentration is substituted to 0.66. From Figure 9 (d), the materials have indirect band gap at the symmetry point of Γ–X. This shows that there is momentum change along the materials. As we observed from Figure 9 (b) and (c) the number of band lines are increasing more below the Fermi level at X = 0.41 and X = 0.66. This is indicates the promotion of the p-type character of the alloy with doping. From table 5, the simulation result indicates that, ZnS is a direct band gap at Γ point with the values of 2.12 eV, but at Γ–X the materials shows indirect band gap with values of 3.83 eV. From this the indirect result seems to have more precision result than the experimental values. This underestimation of the band gap is mainly due to the fact that the simple forms of LDA are not sufficiently flexible to accurately reproduce both exchange correlation energy and its charge derivative [11].

Table 5. Energy band gap (in eV) at the high symmetry points within the Brillouin zone for the conduction band and the valence band of ZnS.

Brillouin	This work	Other Cal.	Experiment
Γ_{16v} - Γ_{1c}	2.12	2.16, 1.96	3.68 [22]
Γ_{16v} –X_{1c}	3.83	3.01 [22]	4.10 [22]
Γ_{16v} - L_{1c}	3.19	3.16 [22]	4.40 [22]
L_{15v} - L_{1c}	4.38	3.38 [22]	4.11 [11]
X_{5v} -X_{1c}	3.08		

Table 6. Energy band gap (in eV) at the high symmetry points within the Brillouin zone for the conduction band and the valence band of BeS.

Brillouin zone	This work	Other Cal.	Experiment
Γ_{4v} - Γ_{1c}	3.73	5.40 [11]	-
Γ_{4v} -X_{1c}	3.03	3.78 [11]	>5.5 [11]
Γ_{4v} - L_{1c}	4.05	5.25 [11]	-
L_{3v} - L_{1c}	4.38	6.46 [51]	-
X_{6v} -X_{1c}	3.52	5.74 [51]	4.86 [51]

As we shown in Table 6, the calculated band structures of BeS (ZB) using LDA schemes gave indirect band gap at Γ–X. In the same trend the calculated band gap is underestimated in comparison with the experimental result with wide band gap and relatively good agreement with the theoretical values.

Table 7. Energy band gap (in eV) at the high symmetry points within the Brillouin zone for the conduction band and the valence band of $Be_{0.41}Zn_{0.59}S$.

Brillouin zone	$\Gamma_{31v} - \Gamma_{1c}$	$\Gamma_{31v} - X_{1c}$	$\Gamma_{31v} - L_{1c}$	$L_{33v} - L_{1c}$	$X_{22v} - X_{1c}$
This work	3.13	3.24	3.67	3.93	3.64

Still the materials are direct band gap at Be concentration X = 0.41 and relatively the range of the direct band gap is increasing as the concentrations of dopant increases.

Table 8. Energy band gap (in eV) at the high symmetry points within the Brillouin zone for the conduction band and the valence band of $Be_{0.66}Zn_{0.34}S$.

Brillouin zone	$\Gamma_{41v} - \Gamma_{1c}$	$\Gamma_{41v} - X_{1c}$	$\Gamma_{41v} - L_{1c}$	$L_{22v} - L_{1c}$	$X_{54v} - X_{1c}$
This work	3.50	3.09	3.85	4.17	3.30

At this concentration the materials have indirect band gap. This shows the contributions of Be concentration.

5.4. Band Structure for rock salt crystal structure

As we observed from the calculated band structures, it is possible to deduced the effects of changing the crystal structures, enhanced the change in electronic properties. In Figure 10 (a), the band structures of the valence and conduction bands overlap. The overlap is caused by a strong lowering of the X_{1c} band with respect to the Γ_{21c} state and by the trend of the LDA method to produce too small values for energy gaps. In the zinc blende phase the X_{1c} band is well above the conduction band minimum, but in the rock salt structure it is shifted to lower energies.

a) b)

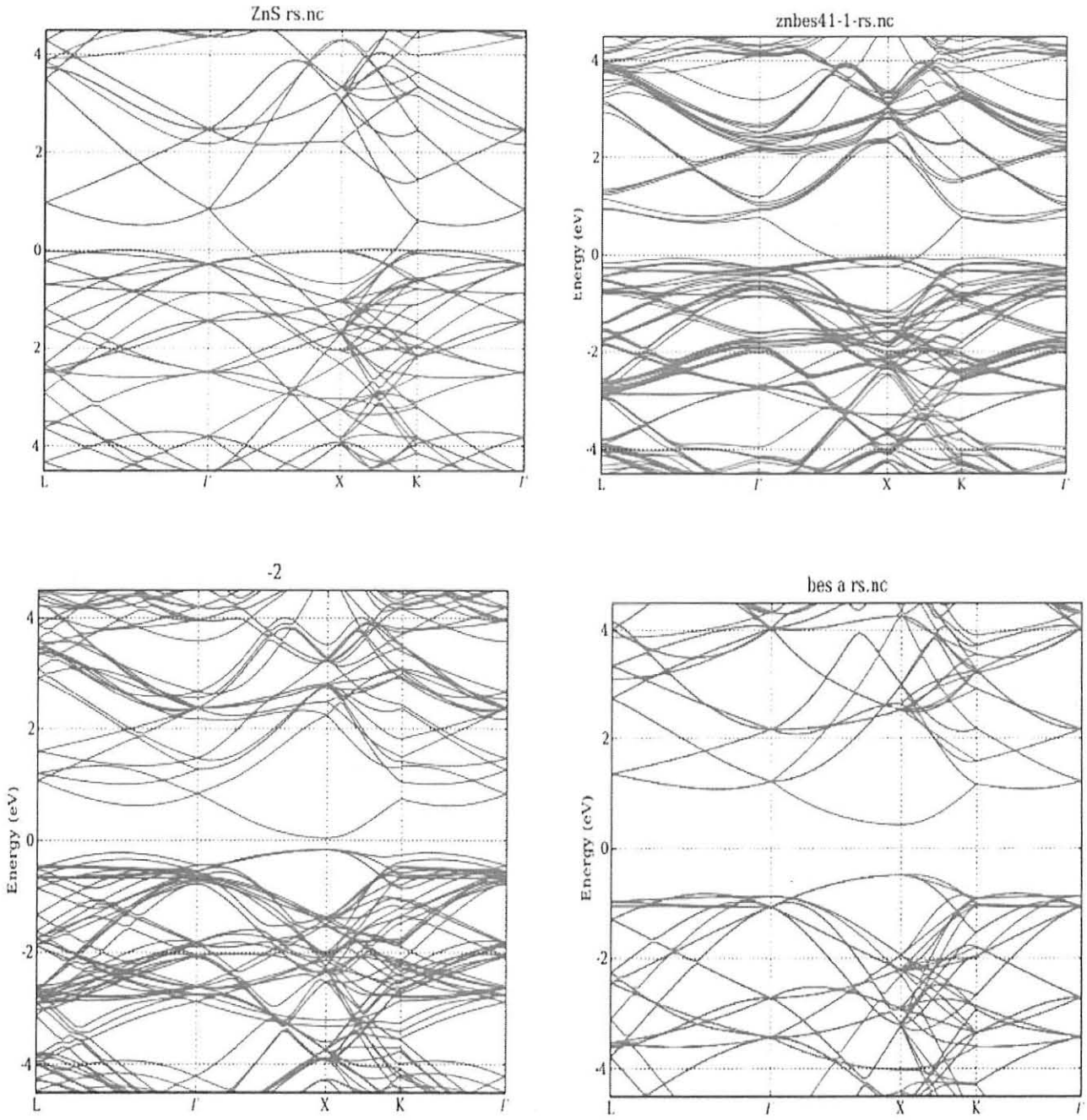

c) d)

Figure 10. Band structures of a $Be_XZn_{1-X}S$ alloy at Be concentrations (X) of a) 0.00 b) 0.41 c) 0.66 and d) 1.00 in the rock salt crystal structure.

The overlapping of materials is observed due to the close packing of the rock salt one, i.e. rock salt has more close packing efficiency than that of the zinc blende one. In doing so, formations of ionic bond are the pronounced. For this reason less energy is required, to excite electron from valence band to conduction band. From Figure 10 (d), it is clearly seen that BeS remains semiconductor. But, it change their symmetry from the indirect between (Γ and X points) to direct band gap (X-X). The reason is that at X- symmetry the coordination's of the crystals have (0.5, 0.0, 0.5), while for ZnS and $Be_{0.41}Zn_{0.59}S$ compounds our study shows metallic phase. But, if we observe the difference among the two compound, as the Be is substituted the number of the energy state is increases. For BeS, the valence band maximum (VBM) and the conduction band minimum (CBM) occurs at the X point, then BeS have direct band gap at this symmetry point as depicted in Figure 10 (d).

Table 9. Energy band gap (in eV) at the high symmetry points within the Brillouin zone for the conduction band and the valence band of ZnS.

Brillouin zone	Γ_{21v} - Γ_{1c}	Γ_{21v} -X_{1c}	Γ_{21v} - L_{1c}	L_{12v} - L_{1c}	X_{26v} -X_{1c}
This work (eV)	1.12	0.89	1.25	0.99	0.00
Other Cal. (eV)	1.84	3.19		-	-
Experiment (eV)	3.80 [51]		-	-	-

Table 9, the band structures for ZnS in the rock salt form shows high symmetry as observed at the (X_{26v} -X_{1c}). This shows that the materials have direct band gap at this symmetry point. From this band gap the materials shows the metallic character due to the overlap of the valence band and conduction band and the values of the gap is 0.00 eV. From this band we observed that the

materials have more band states around the Fermi level. The materials are much closed packed each other; these packing effects enhance or bring the orbital overlapping of the valence band and conduction band.

Table 10. Energy band gap (in eV) at the high symmetry points within the Brillouin zone for the conduction band and the valence band of BeS

Brillouin zone	Γ_{9v} - Γ_{1c}	Γ_{9v} -X_{1c}	Γ_{9v} - L_{1c}	L_{11v} - L_{1c}	X_{16v} -X_{1c}
This work (eV)	2.08	1.29	2.25	2.34	0.91
Other Cal. (eV)	4.21	2.66 [11]	4.25 [11]	-	-
Experiment (eV)	4.50 [11]		-	-	-

Table 11. Energy band gap (in eV) at the high symmetry points within the Brillouin zone for the conduction band and the valence band of $Be_{0.41}Zn_{0.59}S$

Brillouin zone	Γ_{66v} - Γ_{1c}	Γ_{66v} -X_{1c}	Γ_{66v} - L_{1c}	L_{37v} - L_{1c}	L_{37v} - L_{1c}
This work	3.58	3.09	3.85	3.76	3.30

The values of band gap in X = 0.00 and X = 1.00 cases are in reasonable agreement with the theoretical values. It is well known that LDA usually underestimates the energy gap. This is an intrinsic feature of DFT which is not suitable for describing excited state properties. However, it is widely accepted that LDA electronic band structures are qualitatively in good agreement with experiments as regards the ordering of the energy levels and the shape of the bands. However, in this method, the quantities that depend on an accurate description of exchange energy, such as

equilibrium volumes and bulk modulus are in less agreement with experiment. The band gap of $Be_XZn_{1-X}S$ alloy should undergo a direct to indirect crossover at a value of 0.49. For this purpose, we have calculated the direct and indirect band gaps for the alloy at various concentrations.

Table 12. Energy band gap (in eV) at the high symmetry points within the Brillouin zone for the conduction band and the valence band of $Be_{0.66}Zn_{0.34}S$.

Brillouin zone	$\Gamma_{68v} - \Gamma_{1c}$	$\Gamma_{68v} - X_{1c}$	$\Gamma_{68v} - L_{1c}$	$L_{46v} - L_{1c}$	$X_{54v} - X_{1c}$
This work	2.54	0.29	1.32	1.52	0.20

5.5. Gap bowing and its origins

The compute energy band gaps of ZnS, BeS binary compounds, and their alloy $Be_XZn_{1-X}S$ self consistently, LDA are used within DFT. The Calculated results for direct band gaps and indirect band gap in both ZB and RS are given in Figure (9) and (10) respectively. In fact, the LDA functional have simple forms that are not sufficiently flexible to accurately reproduce both exchange correlation energy and its charge derivative. The variation of the direct Γ–Γ and indirect Γ–X band gaps *versus* alloy concentration is given in Figure (11).

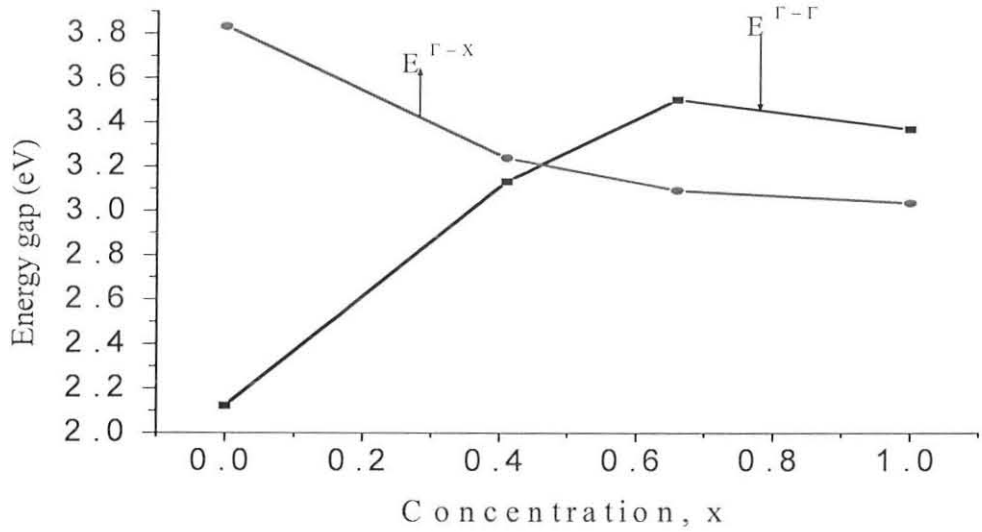

Figure 11. Concentration dependence of the direct (Γ–Γ) and indirect (Γ–X) band gaps in a $Be_XZn_{1-X}S$ alloy Zinc blende.

The direct-to-indirect (Γ – Γ⟶ Γ –X) band gap crossover has been located at a concentration of 0.49 which is slightly close to the FP-LAPW value of 0.76 [4]. In Figure 12 (a), we note that the fundamental gap (Γ–Γ) increases with Be concentration. While in Figure 12 (b), the indirect gap (Γ– X) decreases with Be concentration. The total bowing parameter is calculated by fitting the nonlinear variation, with second order polynomial functions. Using the polynomial fit as shown in Figure 12, we found that our results obey the following variations:

$$E^{\Gamma\rightarrow\Gamma} = 2.11+3.52X - 2.24X^2 \quad (40)$$

$$E^{\Gamma\rightarrow X} = 3.83-1.83X + 1.02X^2 \quad (41)$$

It is shown from the above equations that the variation of the direct (Γ–Γ) and indirect (Γ–X) band gaps as a function concentration has a nonlinear behavior.

a) $E_{\Gamma\rightarrow\Gamma}$ b) $E_{\Gamma\rightarrow X}$

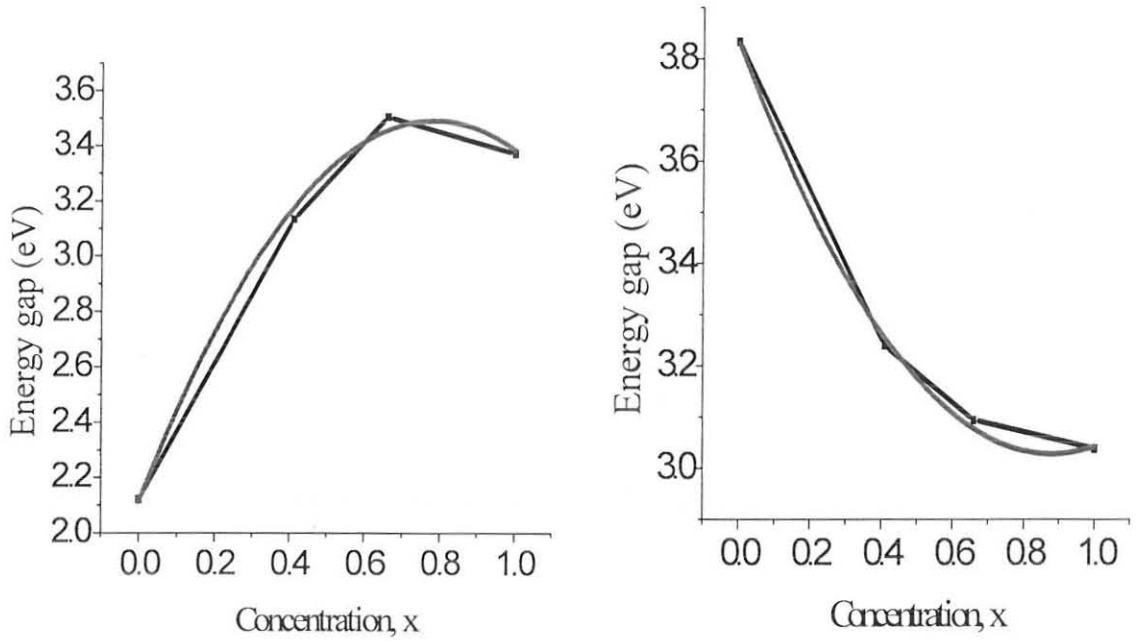

Figure 12. Polynomial fit of the direct (Γ–Γ) and indirect (Γ–X) band gaps *versus* Be concentration (X) of a $Be_XZn_{1-X}S$ alloy Zinc blende.

The obtained nonlinear dependence on concentration (X) by using ab-initio by LDA methods and it is interesting to note that the direct gap (Γ–Γ) *versus* concentration has a downward bowing with a value of 1.02 eV, while the indirect gap (Γ–X) has an upward bowing of -2.24 eV. The values of these bowings are much close to those obtained by using the FP-LAPW method of 1.93 eV and -3.04 eV, respectively [4]. Therefore the band gap bowing is mainly originated from their equilibrium lattice constants to the intermediate alloy value of a (X) that is a clear deviation from the Vegard's rule, due to the large mismatch of the lattice constants between the bulk materials i.e. ZnS and BeS.

5.6. Density of state for the zinc blende crystal structure

Our calculated total density of states (DOS) for different concentrations, i.e. X = 0.0, 0.41, 0.66 and 1.00, of $Be_XZn_{1-X}S$ alloys are given in this part. The DFT calculated DOS spectra for the $Be_XZn_{1-X}S$ alloy are plotted in Figure 13, with the zero of energy corresponding to the Fermi level energy. The calculated DOS spectra in Figure 13, of the binary compounds ZnS, BeS, and their alloy show the type of conductivity of the material. From, Figure 13 (a) for ZnS the DOS peak on the left and right side of Fermi level originate with the spectral positions of ~ -1.35 eV and ~ 0.7 eV, respectively. The value of gap in DOS, which is the gap in between first onset of electron density from the right and left side of the zero point, is found to be similar to the obtained gap energy from the band structure. It is clearly observed that DOS peak for the electrons on upper side of Fermi level shows step increase and reaches maximum value at ~ 3.3 eV. On the other hand, the DOS peak for the hole on left of Fermi level shows small electron density incremental, which are far away from the zero point. This explains the small p–type conductivity of the material. Figure 13 (d) for BeS the DOS peak on the left side of Fermi level originates from the spectral position of ~ - 0.7 eV with a sharp and large onset. On the other hand, the DOS peak for the electrons on upper of Fermi level starts from ~ 2.6 eV with very weak rise of electron density, which is indicative of strong p–type conductivity in the BeS material. From Figure 13 (b) for concentration (X) value of 0.41 the DOS peak on the left side of Fermi level originate from the spectral position of ~ -1.5 eV and shows steep increase and reaches its maximum at ~ -3.5 eV. On the other hand, the DOS peak for the electrons on upper of Fermi level starts from ~ 1.7 eV and shows small values.

a)

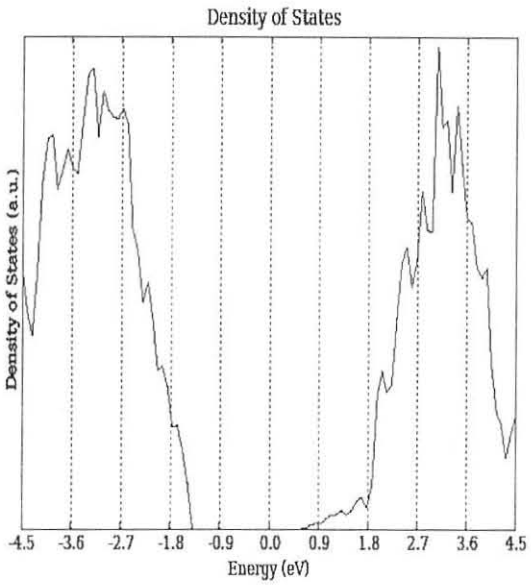

b)

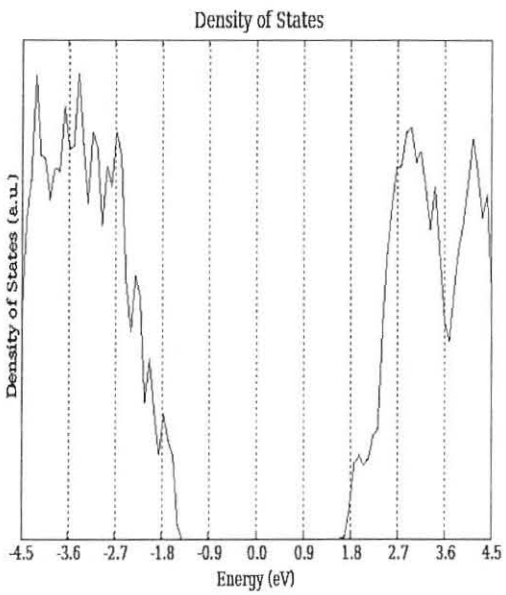

c)

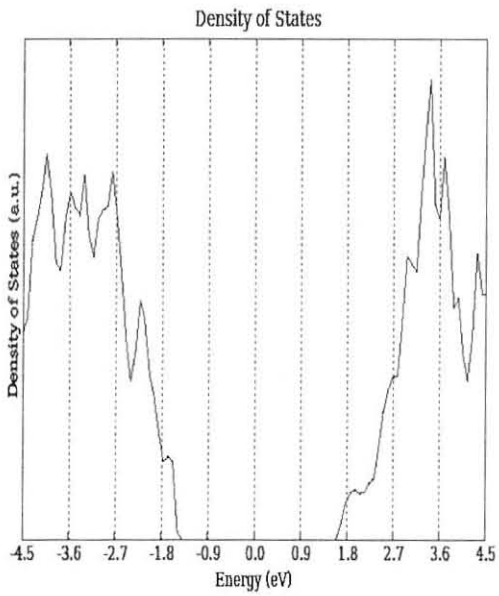

d)

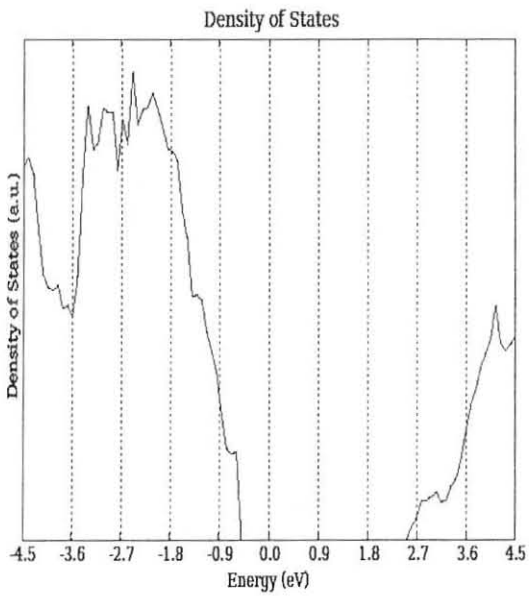

Figure 13. Calculated DOSs for a $Be_XZn_{1-X}S$ alloy at Be concentrations (X) of a) 0.00 b) 0.41 c) 0.66 and d) 1.00.

Effectively DOS peak rises at ~ 2.2 eV. This explains the origin of strong p-type conductivity of the material. Similarly, from Figure 13 (c) for X value of 0.66 the DOS peak on the left side of Fermi level originate from the spectral position of ~ -1.6 eV, shows steep increase, and reaches its maximum at ~ -2.2 eV. On the other hand, the DOS peak for the electrons on upper of Fermi level starts from ~ 1.7 eV and shows small values. Effectively DOS peak rises at ~ 3.2 eV. This again explains the origin of strong p–type conductivity of the 0.66 material. In general, when the lowest conduction bands come closer at the X- point as the alloy is found to be Be rich. This may be a consequence of covalent character of bonding in Be rich alloy. Our calculations also show that the obtained values of gap in DOSs are found to be comparable with their corresponding band structure energies.

5.7. Density of state for the rock salt crystal structure

The typical DOS for the $Be_XZn_{1-X}S$ alloy at Be concentrations (X) of a) 0.00 b) 0.41 c) 0.66 and d) 1.00 are calculated in Figure 14. As seen from Figure 14 (a) and Figure 14 (b) at the right side and left side of the Fermi level are stick together. This stick of the valence and conduction band brings to materials shows metallic character as we observed from the band structure calculation. This indicates that the overall topology of the occupied DOS is similar. For instance, the two lowest conduction bands come closer at the X-point as the alloy becomes Be rich. This may be a consequence of covalent character of bonding in Be rich alloy which will be discussed in the subsequent findings.

a)

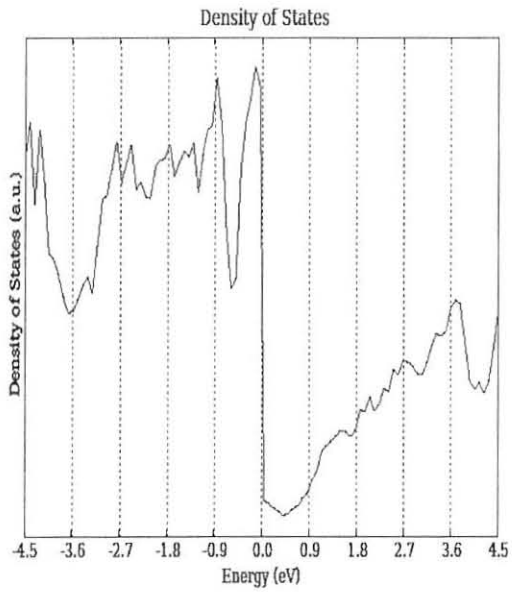

b)

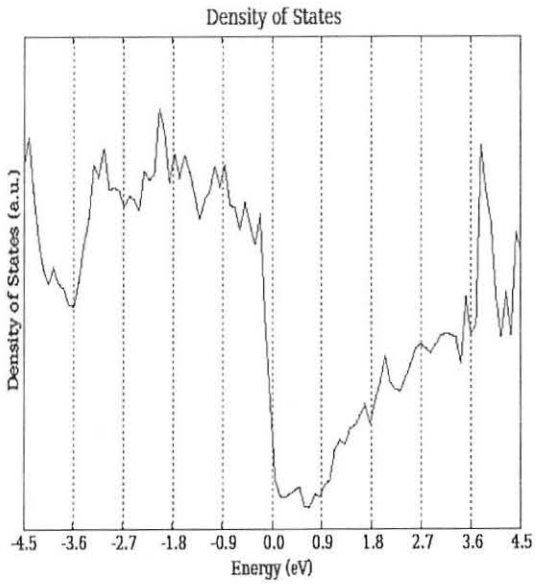

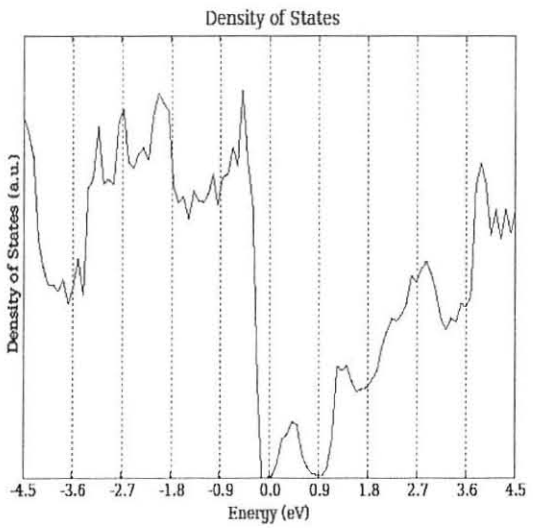

c)

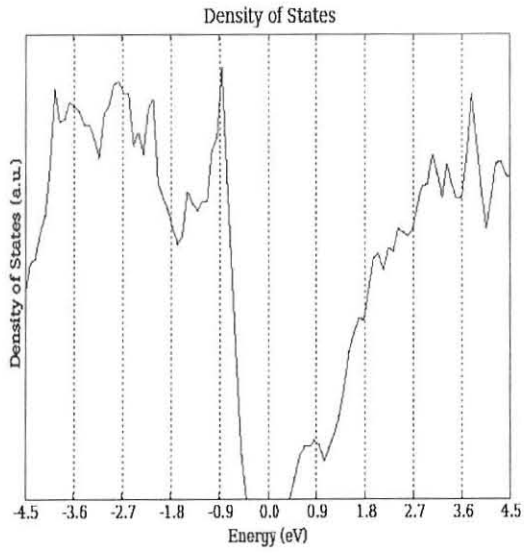

d)

Figure 14. Calculated DOSs for a $Be_XZn_{1-X}S$ alloy at Be concentrations (X) of a) 0.00 b) 0.41 c) 0.66 and d) 1.00.

In Figure 14 (a), there is a sharp spectra increment is observed at 0.00 eV and weak spectra is observed at ~ 0.5 eV. From these spectra the materials have p-type character. In Figure 14 (c) around ~ -0.1 eV there is sharp spectra and many density of states are observed to left sides of the Fermi level, but small spectra is observed at the FWHM of ~ 0.5 eV and at ~ 3.8 eV relatively big spectra is observed. This implies that material shows p-type character. In the same case is phased in Figure 14 (d) at ~ -0.5 eV the onset of the spectra is increasing and rich's ~ -0.9 eV and at ~ 0.5 eV small peak is observed. From this description the materials shows p-type nature. Generally as the crystal structure change from ZB to RS the materials have the tendency to overlap due to densely packing of the crystals. But as the Be substitution increases the overlapping of the somewhat decreases materials increases, as we observed from the spectra of Figure 14 (a) - (d) with and without Be substitution.

CHAPTER 6 CONCLUSIONS AND FUTURE OUTLOOKS

We have presented a systematic density functional theory calculations of structural and electronic properties of ZnS, BeS, and effects of Be substitution on $Be_XZn_{1-X}S$ alloy at the concentration of the Be atoms X = 0.00, 0.41, 0.66 and 1.00 in the ZB and RS phase. We have calculated the concentration dependence of the lattice constant, bulk modulus, pressure derivative, band gap, and density of states by using the modeling of a geometrically relaxed unique supercell of 54 atoms. The total energy has been calculated as a function of unit cell volume and is fitted by Murnaghan's equation of state. The calculated lattice equilibrium and bulk modulus with concentrational variations are found to be in good agreement with the experimental values. As the Be concentration increases the bulk modulus increases slightly and there is small deviation from vegard's law with lattice constant bowing. This deviation mainly due to the mismatch of the lattice parameter between BeS and ZnS. The calculated electronic band structure results show that zinc blende, ZnS, is a direct band gap material and BeS shows indirect band gap materials. The calculated band structure shows a transition from direct band to indirect band gap ($\Gamma \rightarrow \Gamma$) $\rightarrow$ ($\Gamma \rightarrow X$) at X = 0.49. We have additionally predicted that ZnS and BeS compound transforms from ZB (FCC) at ambient pressure to the RS (NaCl) phase at high pressure. It is found that the phase transitions from the ZB structure to RS occur at 22.0 GPa and 61.0 GPa, respectively. Finally, using the as obtained mechanical hardening, we can conclude that a $Be_XZn_{1-X}S$ ternary alloy is useful in the realization of long-lifetime laser diodes by suitably adjusting their Be concentration. As a future extension of current research, the investigations of phonon spectra can be suggested; optical phonon modes of the ternary are expected to get either softened or hardened with Be-dopant concentrations.

REFERENCES

1. Aoumeur-Benkabou, Fatma-Zahra. "Molecular-dynamics simulation of structural and thermodynamic properties of ternary alloy ZnSXSe1-X." Applied Physics Research 3.2 (**2011**):211.
2. Jaffe, J. E., R. Pandey, and M. J. Seel. "Ab initio high-pressure structural and electronic properties of ZnS." Physical Review B 47.11 (**1993**): 6299.
3. Boumaza, A., et al. "First-principles calculations of the structural, electronic, elastic, phase diagram and thermal properties of ZnBeTe ternary alloy." Physica Scripta 86.3 (**2012**): 035703.
4. Hacini, K., et al. "Theoretical study of structural, electronic and thermal properties of ZnBeS ternary alloy." Computational Materials Science 50.11 (**2011**): 3080.
5. Li, Z., et. al. "The Study of Structural Transition of ZnS Nanorods under High Pressure." The Journal of Physical Chemistry C, 115(2) (**2010**): 357.
6. Shinde, M. S., P. B. Ahirrao, and R. S. Patil. "Structural, Optical and Electrical Properties of Nanocrystalline ZnS thin films Deposited by Novel Chemical Route." Archives of Applied Science Research 3.2 (**2011**): 311.
7. Üzar, Neslihan, and M. Çetin Arikan. "Synthesis and investigation of optical properties of ZnS nanostructures." Bulletin of Materials Science 34.2 (**2011**): 287.
8. Pan, Y. W., et al. "Pressure-induced structural transitions of the zinc sulfide nano-particles with different sizes." J. Mater. Sci. Technol 23.2 (**2007**): 193.
9. Yue-Wu, Pan, et al. "Structural phase transformations of ZnS nanocrystalline under high pressure." Chinese Physics Letters 21.1 (**2004**): 67.

10. Mameri, Z., et al. "Pressure effects on the phonon modes in beryllium chalcogenides." Materials Chemistry and Physics 123.1 (**2010**): 343.
11. Haj Hassan, F. El, and H. Akbarzadeh. "Ground state properties and structural phase transition of beryllium chalcogenides." Computational materials science 35.4 (**2006**): 423.
12. Zaoui, A., and F. El Haj Hassan. "Full potential linearized augmented plane wave calculations of structural and electronic properties of BN, BP, BAs and BSb." Journal of Physics: Condensed Matter 13.2 (**2001**): 253.
13. Hassan, F. El Haj, H. Akbarzadeh, and M. Zoaeter. "Structural properties of boron compounds at high pressure." Journal of Physics: Condensed Matter 16.3 (**2004**): 293.
14. Madelung, Otfried. : Semiconductors-basic data", Springer - Berlin, (**1996**).
15. Tamargo, Maria C., ed. 2-6 semiconductor materials and their applications. Vol. 12. Taylor & Francis, (**2002**).
16. Kuskovsky, I., et al. "Photoluminescence characterization of MBE grown ZnBeSe." Journal of crystal growth 214 (**2000**): 335.
17. Guo, S. P., et al. "High crystalline quality ZnBeSe grown by molecular beam epitaxy with Be–Zn co-irradiation." Journal of crystal growth 208.1 (**2000**): 205.
18. Buckley, M. R., et al. "Dielectric functions and critical points of BeZnTe alloys measured by spectroscopic ellipsometry." Applied physics letters 81 (**2002**): 5156.
19. Baaziz, H., et al. "FP-LAPW investigations of ZnBeS, ZnBeSe and ZnBeTe ternary alloys." Physica Status Solidi (b) 243.6 (**2006**): 1296.
20. Ameri, M., et al. "First principles study of structural and electronic properties of BeZnS and BeZnTe alloys." Physica Status Solidi B Basic Research 245 (**2008**): 106.
21. Bafghi, Zhaleh Ghaemi. "SiGe Alloys and Vegard's Law." 7 (**2007**):3529.

22. Ameri, Mohammed, et al. "First Principles Study of Structural and Electronic Properties of OSZn Ternary Alloy." Materials Sciences and Applications 4 (**2013**):63.

23. Singh, Jasprit. "Smart electronic materials: fundamentals and applications." Cambridge University Press, (**2005**).

24. Botti, Silvana, et al. "Long-range contribution to the exchange-correlation kernel of time-dependent density functional theory." Physical Review B 69.15 (**2004**): 155112.

25. Edwards, A. L., and H. G. Drickamer. "Effect of pressure on the absorption edges of some III-V, II-VI, and I-VII compounds." Physical Review 122.4 (**1961**): 1149.

26. Nelmes, R. J., and M. I. McMahon. "Structural transitions in the group IV, III-V, and II-VI semiconductors under pressure." Semiconductors and semimetals 54 (**1998**): 145.

27. McMahon, M. I., et al. "Observation of a simple-cubic phase of GaAs with a 16-atom basis (SC16)." Physical review letters 80.25 (**1998**): 5564.

28. Kumar, Pawan, et al. "Optical, structural and electrical properties of Zinc Sulphide vacuum evaporated thin film." Indian Journal of Pure and Applied Physics 44.9 (**2006**): 690.

29. Qteish, A., and A. Munoz. "Stability and structural properties of ZnS and ZnSe under high pressure." physica status solidi (b) 223.2 (**2001**): 417.

30. Al-Douri, Y., and Ali Hussain Reshak. "Calculated optical properties of GaX (X= P, As, Sb) under hydrostatic pressure." Applied Physics A 104.4 (**2011**): 1159.

31. Bouamama, Kh, K. Daoud, and K. Kassali. "Ab initio calculations in the virtual-crystal approximation of the structural and the elastic properties of BeS(X)Se(1− X) alloys under high pressure." Modelling and Simulation in Materials Science and Engineering 13.7 (**2005**): 1153.

32. Lachebi, Abdelhadi, Mohamed Sehil and Hamza Abid. "First-principles study of cubic B(X)InN alloys." Turk. J. Phys 33 (**2009**): 325.

33. Foulkes, W. M. C., et al. "Quantum Monte Carlo Simulations of Real Solids." High-Performance Computing. Springer US, (**1999**):8787.

34. Kumar, Munish. "Bulk modulus and equation of state of High-Temperature superconductors." physica status solidi (b) 196.1 (**1996**): 209.

35. Zhang, Siyuan, et al. "Calculation of the bulk modulus of simple and complex crystals with the chemical bond method." The Journal of Physical Chemistry B 111.6 (**2007**): 1304.

36. Hann, Michael M., Andrew R. Leach, and Gavin Harper. "Molecular complexity and its impact on the probability of finding leads for drug discovery." Journal of Chemical Information and Computer Sciences 41.3 (**2001**): 856.

37. Tsegaye, Zenebe Assefa. "Density Functional Theory Studies of Electronic and Optical Properties of ZnS Alloyed with Mn and Cr." Thesis, Norwegian University of Science and Technology, **2012**, Retrieved on 15-05-2013 from URL:www.ntnu.diva-portal.org

38. Han, Jeong Woo Liwei Li, and David S. Sholl. "Density Functional Theory Study of H and CO Adsorption on Alkali-Promoted Mo2C Surfaces." The Journal of Physical Chemistry C 115.14 (**2011**): 6870.

39. Kohn, Walter, AXel D. Becke, and Robert G. Parr. "Density functional theory of electronic structure." The Journal of Physical Chemistry 100.31 (**1996**): 12974.

40. Gross, Eberhard KU, and Reiner M. Dreizler, "Density functional theory" Plenum Publishing Corporation, (**1995**).

41. Hohenberg, Pierre, and Walter Kohn. "Inhomogeneous electron gas." Physical Review 136.3B (**1964**): B864.